UNIVERSITAT POLITÈCNICA DE CATALUNYA

ESCOLA TÈCNICA SUPERIOR D'ENGYNIERS DE CAMINS, CANALS I PORTS DE BARCELONA

DEPARTMENT OF GEOTECHNICAL ENGINEERING AND GEOSCIENCES

Coupled analysis of degradation processes in concrete specimens at the meso-level

DOCTORAL THESIS SUBMITTED BY

ANDRÉS ENRIQUE IDIART

SUPERVISED BY:

IGNACIO CAROL

CARLOS MARÍA LÓPEZ

Doctoral Program in Geotechnical Engineering

BARCELONA, MAY 2009

Contents

Abstract

Recent years have witnessed an important shift of the concrete mechanics community towards the numerical study of coupled problems, dealing with environmental-related degradation processes of materials and structures, such as chemical attack, high temperature effects or drying shrinkage.
Traditionally, coupled analyses in the literature have been performed at the macroscale, considering the material as a continuous and homogeneous medium. However, it is well known that the origin of observed degradation phenomena at the material level often lies on the interplay at the level of aggregates and mortar, especially when differential volume changes are involved between material constituents. This is the reason why meso-mechanical analysis is emerging as a powerful tool for material studies, although at present only a few numerical models exist that are able to perform a coupled hygro-mechanical or chemo-mechanical analysis at the scale of the main heterogeneities, i.e. the mesoscale.
This thesis extends the applicability of an existing finite element meso-mechanical model developed within the same research group over the last fifteen years, to the analysis of coupled hygro-mechanical and chemo-mechanical problems, in order to study drying shrinkage and external sulfate attack in concrete specimens. The Voronoï/Delaunay tessellation theory is used to explicitly generate the geometry of the larger aggregates embedded in a matrix representing mortar plus smaller aggregates. Fracture-based interface elements are inserted along all aggregate-matrix and some of the matrix-matrix mesh lines, in order to simulate the main potential crack paths.
The main contribution of the present work is the combination of a coupled analysis with a mesostructural representation of the material, and the simulation of not only crack formation and propagation, but also the influence of evolving cracks on the diffusion-driven process.
Calculations are based on the finite element codes DRAC and DRACFLOW, developed within the research group, which are appropriately modified and coupled together through a staggered approach. The simulations include the evaluation of the coupled behavior, the adjustment of model parameters to experimental data available from the literature, and different studies of the effects of aggregates on the drying-induced microcracking and expansions due to sulfate attack, as well as the simultaneous effect of the diffusion-driven phenomena with mechanical loading. The results obtained agree well with experimental observations on crack patterns, spalling phenomena and strain evolution, and show the capability of the present approach to tackle a variety of coupled problems in which the heterogeneous and quasi-fragile nature of the material plays an important role.

Resumen

En los últimos años, el análisis numérico de problemas acoplados, como los procesos de degradación de materiales y estructuras relacionados con los efectos medioambientales, ha cobrado especial importancia en la comunidad científica de la mecánica del hormigón. Problemas de este tipo son por ejemplo el ataque químico, el efecto de altas temperaturas o la retracción por secado.

Tradicionalmente, los análisis acoplados existentes en la literatura se han realizado a nivel macroscópico, considerando el material como un medio continuo y homogéneo. Sin embargo, es bien conocido que el origen de la degradación observada a nivel macroscópico, a menudo es debida a la interacción entre los áridos y el mortero, sobre todo cuando se dan cambios de volumen diferenciales entre los dos componentes. Esta es la razón por la que el análisis mesomecánico está emergiendo como una herramienta potente para estudios de materiales heterogéneos, aunque actualmente existen escasos modelos numéricos capaces de simular un problema acoplado a esta escala de observación.

En esta tesis, la aplicabilidad del modelo meso-mecánico de elementos finitos, desarrollado en el seno del grupo de investigación durante los últimos quince años, se extiende al análisis de problemas acoplados higro-mecánicos y químico-mecánicos, con el fin de estudiar la retracción por secado y el ataque sulfático externo en muestras de hormigón. La generación numérica de meso-geometrías y mallas de elementos finitos con los áridos de mayor tamaño rodeados de la fase mortero se consigue mediante la teoría de Voronoï/Delaunay Adicionalmente, con el fin de simular las principales trayectorias de fisuración, se insertan *a priori* elementos junta de espesor nulo, equipados con una ley constitutiva basada en la mecánica de fractura no lineal, a lo largo de todos los contactos entre árido y matriz, y también en algunas líneas matriz-matriz.

La aportación principal de esta tesis es, conjuntamente con la realización de análisis acoplados sobre una representación mesoestructural del material, la simulación no solo de la formación y propagación de fisuras, sino también la consideración explícita de la influencia de éstas en el proceso de difusión.

Los cálculos numéricos se realizan mediante el uso de los códigos de elementos finitos `DRAC` y `DRACFLOW`, previamente desarrollados en el seno del grupo de investigación, y acoplados mediante una estrategia *staggered*. Las simula-ciones realizadas abarcan, entre otros aspectos, la evaluación del compor-tamiento acoplado, el ajuste de parámetros del modelo con resultados experimentales disponibles en la bibliografía, diferentes estudios del efecto de

los áridos en la microfisuración inducida por el secado y las expansiones debidas al ataque sulfático, así como el efecto simultáneo de los procesos gobernados por difusión y cargas de origen mecánico. Los resultados obtenidos concuerdan con observaciones experimentales de la fisuración, el fenómeno de *spalling* y la evolución de las deformaciones, y muestran la capacidad del modelo para ser utilizado en el estudio de problemas acoplados en los que la naturaleza heterogénea y cuasi-frágil del material tiene un papel predominante.

Appendix A

In order to integrate the equation that gives the rate of consumption of the *i* different calcium aluminate phases C_i,

$$\frac{\partial C_i}{\partial t} = - k_i \frac{U C_i}{a_i} \qquad \text{for i = 1,n} \tag{A.1}$$

the discretization of the variable U (that represents the sulfates concentration) in time is shown in figure A.1 and done as follows

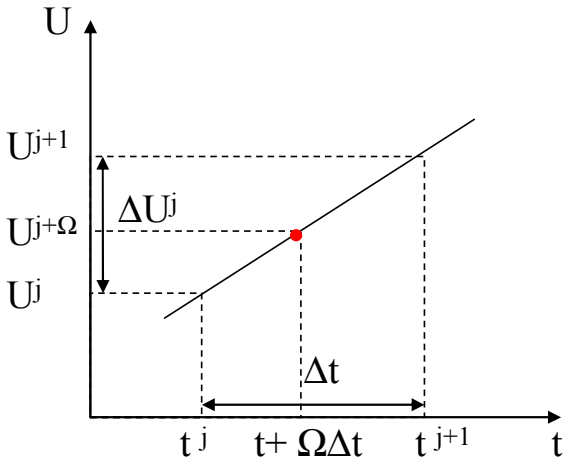

Figure A.1. Linear time discretization.

$$U = U^j + \Omega \Delta U^j, \text{ for } t \in \left[t^j, t^{j+1} \right] \tag{A.2}$$

with $0 \le \Omega \le 1$, and *j* is the iteration number. Plugging in this last expression into the expression A.1 yields

$$\frac{dC_i}{dt} = - k_i \frac{\left(U^j + \Omega \Delta U^j \right) C_i}{a_i} \qquad \text{for i = 1,n} \tag{A.3}$$

or

$$\frac{dC_i}{C_i} = - k_i \frac{\left(U^j + \Omega \Delta U^j \right)}{a_i} dt \qquad \text{for i = 1,n} \tag{A.4}$$

The integration of the previous expression yields

$$\ln C_i \Big|_{C_i^j}^{C_i^{j+1}} = - k_i \frac{\left(U^j + \Omega \Delta U^j \right)}{a_i} t \Big|_{t_j}^{t_{j+1}} \qquad \text{for i = 1,n} \tag{A.5}$$

which may be written as

$$\ln \frac{C_i^{j+1}}{C_i^j} = - k_i \frac{\left(U^j + \Omega \Delta U^j\right)}{a_i} \Delta t \qquad \text{for } i = 1,n \tag{A.6}$$

Finally, C_i^{j+1} can be calculated in an explicit form as

$$C_i^{j+1} = C_i^j \cdot \exp\left\{ -\frac{k_i}{a_i} \cdot \left(U^j + \Omega \cdot \Delta U^j\right) \cdot \Delta t \right\} \tag{A.7}$$

Chapter 1

INTRODUCTION

1.1. Motivation and scope

Over the last few decades, durability of concrete structures has become a key aspect in the design of new structures and the repair of existing ones. A large body of experimental studies can be found in the literature dealing with different kinds of degradation processes, such as chloride ingress, carbonation or sulfate attack. At the same time, simple numerical models based on empirical and phenomenological arguments have been proposed in order to analyze and quantify the rate and extent of specific degradation processes. The main drawback of these simple tools is that the results of the analysis of the diffusion process cannot be directly related to the mechanical response of the specimen or structure, thus rendering their application to real cases somewhat difficult. In recent years, coupled numerical simulations have emerged as powerful tools to study the relation between the diffusion-driven phenomena and the mechanics behind it, and this has been typically done at a macroscopic scale. However, the heterogeneous and quasi-brittle nature of concrete material makes it difficult to study this type of problems assuming a continuous and homogeneous medium. Indeed, damage and fracture in concrete are generally governed by the main heterogeneities in the material, and the influence of cracks in the different diffusion processes cannot be neglected in general. To remediate this, and with the help of rapidly increasing computer resources, mesomechanical analyses have recently emerged and proved to be very helpful in understanding the macroscopic behavior of concrete starting from the more fundamental response of its individual components.

All the specific features described above, which are characteristic of cementitious materials, have motivated the present work, which deals with coupled numerical simulations of drying shrinkage (hygro-mechanical coupling) and external sulfate attack (chemo-mechanical coupling) in concrete specimens within a mesostructural framework. In the case of drying shrinkage, the main interest is in evaluating the effect of drying-induced microcracks and the material heterogeneity on the overall response of concrete specimens in terms of strains, weight losses, moisture distribution and crack patterns. The case of sulfate attack is more complicated from a chemical point of view, but also from a mechanical one, since experiments have shown very large expansions and spalling phenomena leading to total disintegration in some extreme cases. Recent advances in the experimental and also in the modeling fields have shown encouraging results towards a scientific interpretation of the main processes involved, a generally accepted explanation of the overall process is still missing. This degradation process is studied with the present approach in order to reflect the correct levels of expansion and

crack patterns starting from a diffusion process for the sulfate ingress and considering the main chemical reactions which take place.

1.2. Objectives

The main objective of this thesis is to develop a 2D numerical model for the study of coupled problems in concrete involving diffusion-driven phenomena and mechanics from a mesostructural point of view. Secondly, the model has to be verified with existing experimental data and analytical solutions. The primary focus has been made on the drying shrinkage and external sulfate attack problems in concrete specimens. The goal has been to reproduce numerically the overall response of saturated specimens, subjected to drying or submerged in sodium sulfate solutions, in terms of evolution of strains, crack patterns and/or weight losses. As the starting point, an existing meso-mechanical model for concrete in 2D, and the FE codes `DRAC` and `DRACFLOW`, for the mechanical and diffusion analyses, respectively, developed by the Mechanics of Materials group at UPC, have been used. In order to achieve the main goal, various requirements had to be fulfilled, which are listed in the following:

- The geometry and mesh generation procedure in 2D for concrete specimens has to be fully automated and considerable improvements of several features must be introduced, allowing the generation of more complicated geometries, with notches and wedges, and a greater freedom in the aggregate distribution and sizes than in the original mesh generation tool, the adaptation of meshes to diffusion problems (mesh refinement near the exposed surface/s). Also the quantification of microcracks during the post-processing stage is an important aspect that has to be considered.
- The constitutive model for zero-thickness interface elements that accounts for the aging effect has to be updated. More specifically, the numerical integration scheme and the consideration of a consistent tangent operator have to be addressed, and improvements in the convergence must be achieved for more computational demanding cases.
- A model for studying drying shrinkage in concrete within the mesostructural framework has to be developed and many features have to be examined, such as the formulation of the shrinkage coefficient or the moisture capacity matrix. Also the effects on the drying process of a single crack and a single aggregate with changing characteristics should be studied.
- A model for analyzing the diffusion-reaction process taking place in the external sulfate attack problem in concrete has to be developed. From an extensive literature review, the most appropriate existing model must be adopted and adapted to the present mesostructural framework with discrete cracking. Also, the possibility of improvements in the formulation is to be considered. The diffusion of ions through open cracks has to be addressed and numerically quantified.
- One of the most important aspects is the simulation of different degradation scenarios, with different boundary conditions, different material properties and aggregate volume fractions, and eventually evaluating the model also under simultaneous mechanical loads.

- The introduction of new material parameters for the coupled calculations and the fact that simulations have been performed in 2D make it difficult to verify the model. Thus, adjustment of model parameters with experimental results is an important task that has to be addressed during the course of this thesis.

1.3. Methodology

In order to perform a coupled hygro-mechanical (H-M) or chemo-mechanical (C-M) finite element (FE) analysis of concrete at the meso-level an explicit two-dimensional (2D) representation of its internal structure is carried out. Only the largest aggregates are discretized in the FE mesh and are embedded in a matrix phase representing the mortar plus smaller aggregates. This is motivated by the fact that fracture and failure in concrete are generally governed by the main heterogeneities in the material. The geometry of the discretized aggregates is numerically generated by using the standard Voronoï/Delaunay tessellation theory, allowing the representation of the effect of formwork walls on the numerical specimen surfaces. Zero-thickness interface elements are inserted *a priori* between all the aggregate-matrix contacts and also along some predefined matrix-matrix contacts in order to represent the main potential crack paths. From a mechanical point of view, these elements are equipped with an elasto-plastic constitutive model and the evolution of the fracture surface is governed by fracture mechanics-based parameters. The continuum elements are assumed to behave linear elastically or visco-elastically with aging, depending on the case studied. Thus, the non linearity of the model is achieved exclusively by means of the zero-thickness interface elements. The diffusion analysis for drying or sulfate ingress is performed over the same FE mesh, allowing the consideration of the diffusive properties along the micro/cracks, in addition to the diffusion through the continuum. These features make the present model a powerful tool for the analysis of coupled problems in heterogeneous and quasi-brittle materials. Relative humidity is considered as the only variable governing the moisture diffusion in the drying shrinkage simulations. In the case of modeling of external sulfate attack, a diffusion-reaction equation for the sulfate ions ingress, with a second-order reaction, is considered, and reaction kinetics is explicitly introduced. The coupling between mechanics and diffusion-driven phenomena, which are calculated separately by two (in principle) independent codes, is materialized with the use of a staggered approach. Iterative coupling is only needed when diffusion through the cracks is to be considered. Otherwise a simple uncoupled calculation suffices, in which the results from the simulation of the diffusion process, in the form of shrinkage strains or thermal-like expansions, serve as input to the mechanical analysis, where the overall response is determined. Finally, time discretization is performed through a finite difference scheme.

1.4. Organization of the thesis

After this short introduction, this thesis is structured as briefly described in the following paragraphs.

Chapter 2 reviews the existing mesostructural models and describes in some detail the numerical approach used in this thesis for the modeling of concrete and other cementitious materials at the meso-level. First, the various levels of analysis are introduced, and the different numerical models at the meso-level developed in the past are compared, with emphasis not only on the mechanical performance, but also on recent work done in the domain of coupled problems at this scale, more specifically

aiming at diffusion-driven phenomena coupled with mechanics. Next, existing crack modeling strategies are briefly described and the constitutive model for interface elements that accounts for aging effect used in this thesis is presented. Finally, the mesh generation procedure in 2D and the description of the aging viscoelastic behavior of the model are addressed.

Chapter 3 reviews the state-of-the-art regarding drying shrinkage and the fundamentals of creep in concrete, with emphasis on the former of these two common concrete topics. The most important experimental features are described and the up-to-date available modeling tools are critically assessed. Special attention is given to the shrinkage-induced microcracking and its detrimental effects on mechanical properties, but also on the transport and diffusive properties. The effect of the presence of aggregates on microcracking is discussed as well.

In Chapter 4, the main results obtained regarding the modeling of drying shrinkage in concrete specimens are presented. The first two sections describe the diffusion model in detail, for the continuum as well as the microcracks, and the coupling strategy. Next, results on the effect of a single crack on the drying process and of a single inclusion on the internal microcracking are presented. The coupled hygro-mechanical analysis at the meso-level is addressed, with detailed studies of the effect of aggregates on the drying-induced microcracking and the adjustment of model parameters with experimental results on drying shrinkage of concrete specimens (Granger, 1996). Finally, drying shrinkage simulations under a simultaneous compression load is considered.

Chapter 5 includes a review of the experimental evidence of the external sulfate attack problem in concrete and concrete structures. The chemical reactions involved, the factors affecting the extent of degradation and the different kinds of sulfate attack are briefly described. Next, a review of the proposed models found in the literature and their critical assessment are presented. Models for the chemo-transport problem of sulfate ingress as well as the mechanical analysis of sulfate attack have been studied in detail, and an overview of the main advantages and drawbacks of the different procedures is performed.

In Chapter 6, the most relevant results of the modeling of external sulfate attack of concrete specimens under saturated conditions are presented. The first sections describe in detail the model developed and present the verification of the numerical implementation with analytical formulas. Next, the application to the cases of mortar bars under sodium sulfate attack and the study of the influence of the aggregate size on the microcracking due to matrix expansions are presented. The coupled C-M analysis of concrete at the meso-level is addressed, and the influence of some material parameters and the effect of coupling are studied. In addition, the adjustment of some model parameters with experimental measurements of expansion of concrete specimens under external sodium sulfate attack is included.

Finally, Chapter 7 summarizes the main conclusions that can be drawn from this thesis, as well as the possible directions for future work, in the field of coupled problems and mechanical analysis of quasi-brittle materials.

Chapter 2

MESOSTRUCTURAL MODELING

Computational modeling of damage and fracture of quasi-brittle materials, such as concrete, is a challenging task. Since the beginning of numerical analysis via Finite Elements in the early 70s, this has been traditionally done using the macroscopic approach, i.e. considering concrete as a homogeneous material, and its intrinsic behavior described by continuum-based constitutive models. However, already in the 80s and mainly in the 90s, that approach started showing some important limitations and in the last decade a lot of effort has been devoted to take into account the material microstructure at different scales of observation. In this chapter, focus is made on the proposed models for studying concrete from a mesostructural viewpoint, in which only the main heterogeneities of the material (i.e. the larger aggregates) are explicitly represented. Accordingly, the chapter is organized as follows. First, the various scales of observation commonly considered in material analysis (macro, meso, micro and nano) are introduced. Next, the different types of meso-scale models are discussed and compared, with emphasis not only on the mechanical performance but also on what has been done so far regarding the coupled hygro-mechanical or chemo-mechanical behavior of concrete at this scale. A brief discussion on the generation of geometries at the meso-level is presented, together with a description of the process to obtain the FE meshes for the simulations included in this thesis. The main crack modeling strategies are then addressed, and different mechanical constitutive models especially designed for zero-thickness interface elements are discussed. Finally, the interface model used throughout this thesis, that considers the aging effect, is described in detail.

2.1. Levels of analysis

Although concrete is a heterogeneous material obtained by mixing cement, water and aggregates of different sizes, sometimes up to several centimeters, traditional engineering studies have considered concrete as a homogeneous material that can be idealized as an infinitesimal continuum medium with average properties. This may be called the *macroscopic approach* (figure 1a). In the early 80's, Wittmann (1982) proposed three levels of observation for concrete studies, from lower to higher: the microscopic level at the micro-meter scale (μm), the mesoscopic level at the mm-cm scale, and the macroscopic level at the metric scale (figure 1). At the macro-level, most of the models proposed in the literature consider phenomenological relations based on macroscopic observations, typically between average strain and average stress on a sufficiently large concrete volume. Despite the oversimplification that this implies, this approach, linked to the use of continuum-type constitutive models such as plasticity and/or damage theory plus, in some cases, some principles of fracture mechanics, has

led to a relatively satisfactory description of the basic features of the mechanical behavior of concrete. This is however at the price of increasing the complexity of the constitutive models, with many physically-meaningless ad-hoc parameters and functions.

The drastic increase in computer power over the last two decades made it possible to start introducing explicitly the first-order material heterogeneities in the analysis (i.e. the larger aggregates in the case of concrete or the sand particles in the case of mortar; figure 1b,c). This approach, initially done only for small material specimens, provides a much more powerful and physically-based description of the material behavior in general, and specifically of the fracture processes and mechanical properties of concrete. To a certain extent, this could be expected, since we know that the apparent macroscopic behavior observed macroscopically is a direct consequence of the more complex intricate phenomena that take place at the level of the material heterogeneities. In the case of concrete, the components considered are typically the larger aggregates, the mortar, and the interfaces between these two. The model proposed in this study is included in this category. The advantage that compensates the higher computational cost of performing such an analysis is the resulting simplification of the models that have to be used to represent the behavior of each component present in the heterogeneous material.

A third scale of analysis is the microscale (figure 1d left), in which the internal structure of the hardened cement paste (HCP) or the interfacial transition zone (ITZ) are studied. Chemical processes during hydration, drying or attack of an aggressive agent are important features at this level. Enormous advances have been achieved in this field, resulting in the development of more resistant and durable concretes. Additionally, the development of new experimental techniques, such us nanoindentation or transmission electron microscope (TEM), has permitted to study concrete at a lower scale: the nanoscale, which could be considered a fourth level of analysis (figure 1d right). One of the many applications at this scale aims at determining the composition and behavior of the calcium silicate hydrates (CSH), something that is emerging as a topic of major importance in concrete technology, since this reaction product turns out to be responsible, to a large extent, of the overall mechanical and time-dependent properties of concrete.

In a multiscale analysis the results obtained from one scale should provide input information for the upper level. For instance, in the case dealt with in this thesis, microstructural studies should give information on the behavior of the matrix or the interfaces at the mesoscale, and the results obtained at the latter should provide insight into the macroscopic behavior (Willam *et al.*, 2001). This requires the determination of the minimal representative volume element (RVE) at each scale of the concrete material. It has been shown that the determination of such a volume at the concrete mesoscale is not straightforward and that it depends on many factors, such as periodicity of aggregates distribution and boundary conditions, ratio between matrix and aggregate stiffness, etc. (see Gitman *et al.*, 2007 and references therein). Given the difficulty of this determination, and the high computational cost, one may wonder why we need to perform an analysis at the meso-level. By performing such an analysis we are restricting ourselves, due to a high computational cost, to the simulation of concrete lab specimens or small concrete members at the most. The main advantage of mesostructural studies is the fact that simpler models, as compared to a macroscopic one, may be used for each of the components defining the heterogeneous material. In the case of concrete, the aggregate and mortar phases as well as the interfaces between

them have a life on their own. It has been shown that with the use of such an approach, the resulting overall complex behavior of concrete specimens comes out naturally as a result of using simple models for each of the phases (see e.g. López, 1999, López *et al.*, 2008 or Caballero *et al.*, 2006). Moreover, the effect of different aggregate materials, distributions and/or shapes (or even with the addition of fibers, see e.g. Leite *et al.*, 2004 and Li *et al.*, 2006) can be studied in a more direct and systematical way than with the use of homogeneous models at the macro-scale.

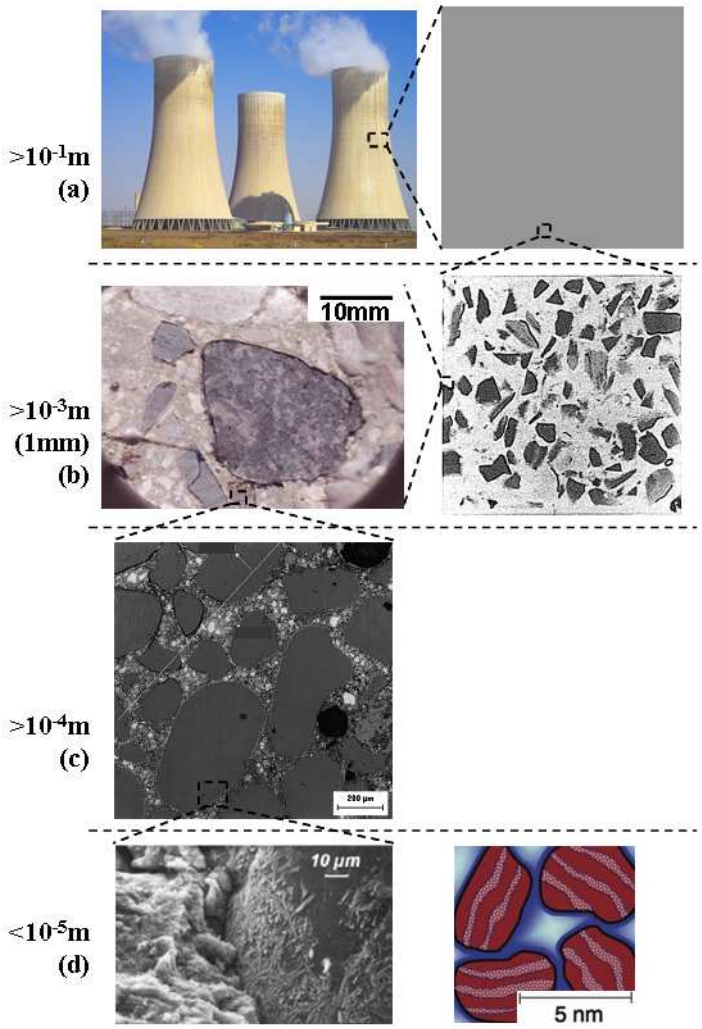

Figure 2.1. Representation of different levels of analysis. (a) Macroscale; (b) concrete mesoscale; (c) mortar mesoscale; (d) micro and nano scales.

2.2. Numerical models at the meso-level

Even though mesostructural models have become popular only over the last decade, there exist in the literature a number of previous proposals dealing with continuous and lattice representations of the heterogeneous medium, starting with the pioneering continuum model named "*béton numérique*" by Wittmann and coworkers (Roelfstra *et al.*, 1985), and other models that followed in subsequent years (Stankowsky, 1990; Bazant *et al.*, 1990; Schlangen & van Mier, 1992; Vonk, 1992; de Schutter & Taerwe, 1993; Wang & Huet, 1993).

Most of the models at the meso-level proposed in the literature focus their attention on the study of crack patterns and stress-strain curves under purely mechanical loading of concrete specimens, and only a few of them have extended their applicability to the analysis of coupled degradation processes, such as hygral gradients (Sadouki & Wittmann, 2001; Schlangen *et al.*, 2007), thermo-mechanical problems (Willam *et al.*, 2005) or chemical attack. This is to some extent surprising since some of the early models mentioned above had already proposed to study the drying behavior of composites at this scale (Roelfstra *et al.*, 1985 and more recently upgraded to preliminary analysis of drying of 3D samples in Hörsch & Wittmann, 2001; Tsubaki *et al.*, 1992; Sadouki & van Mier, 1997), as can be seen in figure 2.2. For instance, Guidoum (1993) studied the viscoelastic response of concrete with a 3D composite model with ellipsoidal inclusions subjected to uniform shrinkage strains of the matrix, obtaining rather crude approximations (cracking was not considered in the simulations). In (Tsubaki *et al.*, 1992), a smeared crack approach is introduced in the meso-level simulations, with very regular and coarse particle (represented by circles) distribution, to study drying shrinkage. Although the simulations were very qualitative, they identified internal cracking around the aggregates, in agreement with experimental observations (see Chapter 3).

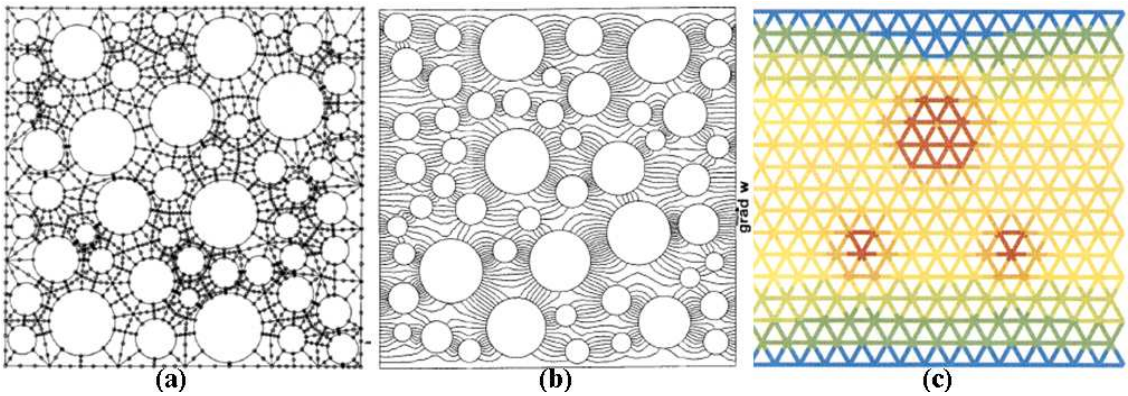

Figure 2.2. Mesostructural representations of the drying process of a composite: (a) special FE mesh for moisture diffusion in concrete and (b) results presented as iso-hygral curves (from Roelfstra *et al.*, 1985); (c) typical moisture distribution in a lattice model, showing saturated aggregates and dried matrix (Schlangen & van Mier, 1997).

To the author's knowledge, there does not seem to be in the literature any continuum-based model at the meso-level able to tackle coupled analysis of concrete using exactly the same finite element mesh for the mechanical and the moisture diffusion analyses. A meso-level study of the alkali-silica reaction has been recently proposed (Comby, 2006), although the FE analysis was purely mechanical, and no transport model seems to have been included in the analysis.

As already pointed out, there is nowadays a large number of different mesomechanical models dealing with the geometry generation and meshing algorithms in very different ways. Most of them may be included into the following three broad groups of meso-models: continuum-based, lattice type and particle models. As it may be expected, they all have their advantages and disadvantages, and in the following a brief review and comparison is given.

2.2.1. Lattice models

Lattice models are characterized by a grid of rod elements, generally forming triangular shapes (Schlangen & van Mier, 1992; Bolander *et al.*, 1998; Lilliu & van Mier, 2003; van Mier & van Vliet, 2003; Grassl *et al.*, 2006), but also with a rectangular scheme (Arslan *et al.*, 2002; Ince *et al.*, 2003; Leite *et al.*, 2004), which represents the continuous medium in a simplified manner (see figures 2.3 and 2.4). These rod elements are able to transfer moments, axial and shear forces. In order to obtain the final finite element meshes, any desired geometry may be superimposed on top of the grid, thus defining different mechanical properties for rods falling in the aggregate, matrix or interface (between the two) domains, as shown in figure 2.3a,b. This method yields a great freedom for aggregate distribution and shapes. Although any aggregate shape could in principle be superimposed, circular (2D) or spherical (3D) shapes have been preferred in the literature, thus neglecting any aggregate angularity effect (Schlangen, 1993; Bolander, 1998; van Mier *et al.*, 2002; Leite *et al.*, 2004). An advantage of adopting such a shape is that a statistical analysis may be performed to extract a 2D representation of a given three dimensional aggregate distribution, like for instance the Fuller curve (Walraven, 1980).

One of the main disadvantages of the lattice representation is an imperfect shape of the resulting stress-strain curves (see figure 2.3c) showing sharp drops due to beam removal (when tensile strength is reached), although some improvements have recently been made in this respect (Ince *et al.*, 2003). Also, the element removal strategy usually employed to simulate cracking does not account for possible crack closure, and does not guarantee in general calibrated fracture energy consumption. Another drawback is that the length of the beam elements has to be smaller (approximately by three times, see Schlangen, 1993) than the smallest aggregate represented in the mesh, thus increasing considerably the number of degrees of freedom in the calculation (see also figure 2.4a). It should be noted that the elastic properties of the composite strongly depend on the regularity of the lattice scheme (van Mier, 1997), yielding for example a zero Poisson's ratio for a regular square lattice.

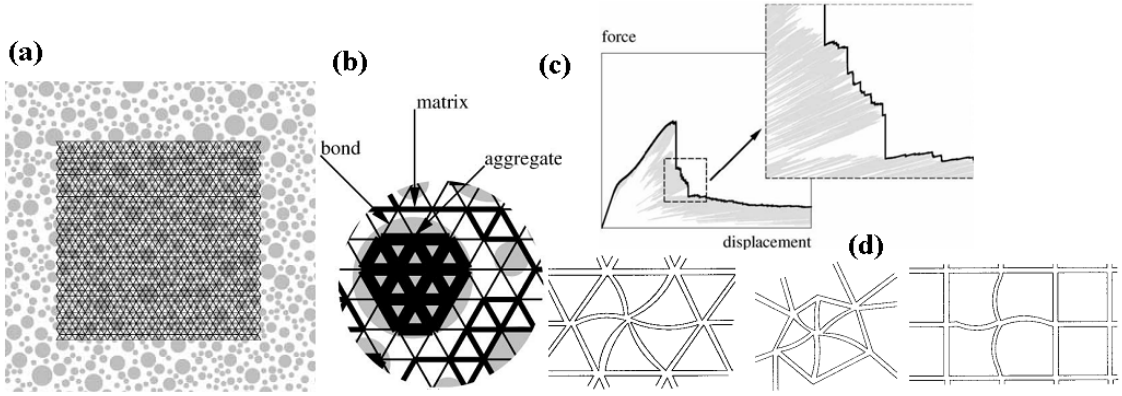

Figure 2.3. Lattice model main features: (a) overlaying of a triangular lattice on top of a circular aggregate array geometry; (b) identification of material law assigned to each beam element; (c) typical smoothening of a force–displacement diagram obtained from a lattice simulation; (d) different lattice types (a, b & c taken from Lilliu & van Mier, 2003, and d from Ince *et al.*, 2003).

Finally, despite reasonable approximations have been achieved for the moisture diffusion uncoupled analysis in concrete or mortar by considering lattices as conductive

pipes (Sadouki & van Mier, 1997; Jankovic *et al.*, 2001; Jankovic & Wolf-Gladrow, 2006), its applicability to diffusion-reaction problems has not been tested, and the introduction of the influence of cracks on the diffusion process has not been attempted and does not seem straightforward.

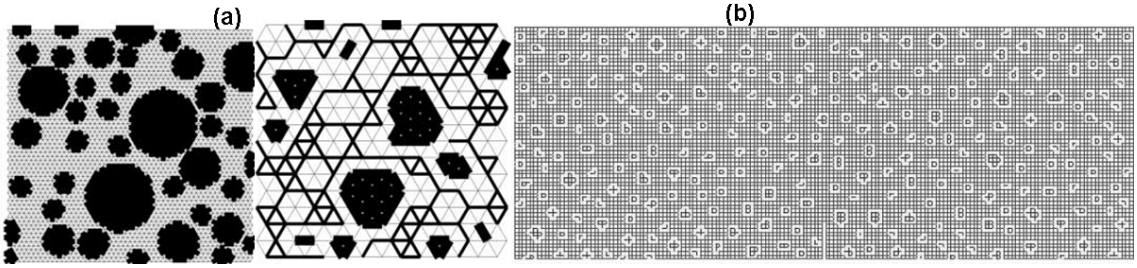

Figure 2.4. Lattice representation of the continuous medium. (a) Comparison of two lengths of beams in a triangular lattice representing the same geometry (van Mier *et al.*, 2002); (b) concrete mesh represented by a square lattice grid (Ince *et al.*, 2003).

2.2.2. Particle models

This type of model seems to have been first introduced for concrete by Bazant and coworkers (Zubelewicz & Bazant, 1987; Bazant *et al.*, 1990), based on some ideas of the *Distinct Element Method* (DEM), proposed earlier for the study of granular geomaterials (Cundall & Strack, 1979). From the viewpoint of the resulting numerical analysis, the nature is similar to the lattice models described in the previous section, in the sense that in both cases the resulting system is a reticulate beam structure. It is for this reason probably, that some particle models have been recently presented in the literature under the hat of *lattice models* (Cusatis *et al.*, 2006), although in the present case each lattice node corresponds to the center of one aggregate, and each beam represents the behavior of the contact between two particles, therefore with a very different meaning than the original lattice models described in the precedent section (this is why the terminology of "particle model" seems preferable, while the choice of the term "lattice" seems in this case unfortunate and even misleading). The *particle* approach may be in general imagined as a random distribution of rigid particles, corresponding to the aggregates (figure 2.5), separated by deformable interfaces equipped with constitutive laws formulated in terms of forces *vs.* displacements (figure 2.5a,b), with a perfect brittle or softening behavior (Bazant *et al.*, 1990; Jirásek & Bazant, 1995; Cusatis, 2001; Cusatis *et al.*, 2003; Cusatis *et al.*, 2006). Other authors use similar methods although the "particles" do not necessarily correspond to physical aggregates, but to sub-domains randomly generated within the specimen or structure, for instance using Voronoï/Delaunay theory. This is the case of the rigid-body spring models (RBSM), which are included in this category (Kawai, 1978; Bolander & Berton, 2004; Berton & Bolander, 2006; Nagai *et al.*, 2004), where zero-size springs are placed along the boundary segments of rigid interconnected elements (figure 2.5c). Note however, that, since the nodes are located at the particle centers, and the shear-normal constitutive laws are established at some point at mid-distance between them, in particle models the resulting constitutive laws for the beam may turn out complex constitutive relations involving normal forces, shear forces as well as moments (and in 3D, perhaps even also torsional forces).

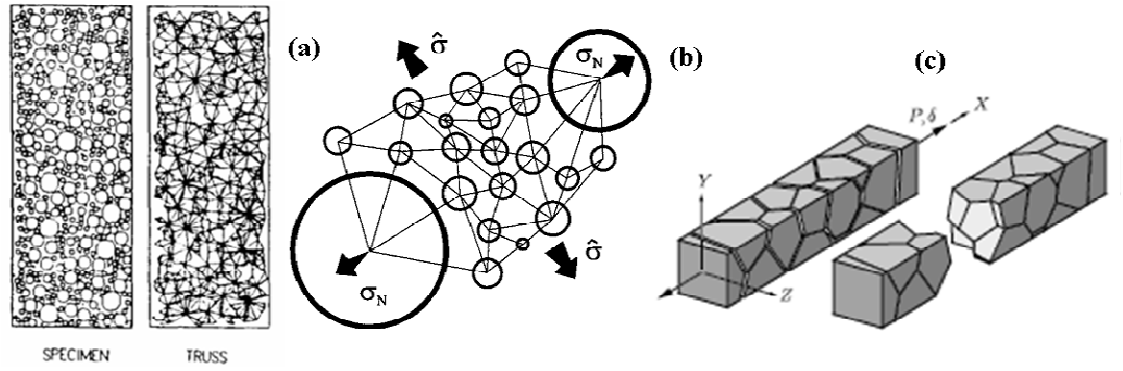

Figure 2.5. Classical representation of particle models. (a) Typical arrangement of circular aggregates and their corresponding truss members (from Bazant *et al.*, 1990); (b) detail of connection between particles and trusses (from Cedolin *et al.*, 2006); (c) typical crack pattern of RBSM under uniaxial tension (from Berton & Bolander, 2006).

The main advantage of these particle models is that they are not as computationally expensive as the continuum-based models (see next section), although at the expense of a simplification of the mechanical problem.

There are, however, also some drawbacks. A first one is of the conceptual type: the main advantage of meso-level models with respect to macroscopic continuum analysis (which is that by considering the more complicated meso or micro geometry, the ingredients of the model and in particular the constitutive material laws, should be simpler) may be partially lost. In effect, in the particle models the fictitious beam constitutive model involving all 3 cross-sectional forces in 2D (or 6 in 3D) may be no simpler (or in many cases, considerably more complicated and less physical) than the traditional phenomenological constitutive laws for the macroscopic equivalent homogeneous continuum.

Another disadvantage of particle models for concrete consists of the crack paths which may be obtained. As pointed out before, the potential cracks in this approach basically correspond to the contact planes between particles, which are in principle perpendicular to the model "beams". This may lead to crack patterns with relatively unrealistic crack roughness at large scale (see for instance figure 2.5c from Berton & Bolander, 2006). Under tensile-dominated loading, this artificial roughness may not have a significant effect on the resulting overall load-displacement curves. In compression behavior, however, small differences in roughness (and also apparently minor details of the constitutive law) may have large effects on the overall response, often leading to ever-increasing load-displacement curves, or, if this effect is compensated by introducing a compressive failure of the beams ("crushing"), to unrealistic microcrack patterns and incorrect lateral expansion or dilatancy effects (i.e. volumetric curve in uniaxial compression test). This deficiency has been in fact recently recognized by the original authors of the DEM, who have proposed new updated versions of the approach in which additional shear-compressive failure lines or mechanisms are superposed to the original particle structure in order to allow for the right compression failure kinematics to develop in the overall boundary-value problem (Cundall, 2008).

Finally, also the extension of particle models to diffusion-based phenomena has to be mentioned. The particle model proposed by Bazant and coworkers has not been yet extended to coupled problems, although time-dependent phenomena as creep in concrete has been studied (Cusatis, 2001). The RBSM has been coupled with a random

lattice model for moisture movement, even though the analysis performed was uncoupled, *i.e.* not considering the influence of cracking on the drying process (Bolander & Berton, 2004). In a more recent study within the framework of the RBSM (although not at the meso-scale), a coupled analysis considering the effect of cracks on transport processes has been proposed (Nakamura *et al.*, 2006). There is an evident increase in the level of complexity of the model, since in this case two systems of truss networks (in addition to the continuum Voronoï particles for the mechanical analysis), one for the transport through the bulk concrete and the other for the flow through cracks, have to be added for a correct representation of the coupled process.

2.2.3. Continuum models

The last family of mesostructural representations is the continuum-based models. Most of the early models at this scale belong to this group (Roelfstra *et al.*, 1985; Stankowsky, 1990; Vonk, 1992; de Schutter & Taerwe, 1993; Wang & Huet, 1993 and 1997), and also the one which is the basis of this thesis (López, 1999; Caballero, 2005). During recent years, a considerable number of scientific groups have developed continuum models for studying either the meso-scale of concrete (Wang *et al.*, 1999; Tijssens *et al.*, 2001; Wriggers & Moftah, 2006; Häfner *et al.*, 2006; Comby, 2006; Puatatsananon *et al.*, 2008), mortar and cement paste and its pore structure (Bernard *et al.*, 2008), and other composites with ellipsoidal inclusions (Zohdi & Wriggers, 2001; Romanova *et al.*, 2005). One of the main advantages of these models is that they represent composite materials in a more realistic fashion, considering continuum fields of the state variables outside the cracking zone (figure 2.6). This is a powerful feature, as compared to other meso-models, especially when diffusion-driven phenomena and chemical reactions are to be analyzed. Another big advantage is that constitutive models really get simplified in this case, consisting in the simplest case of the normal-shear cracking laws along interface lines. Critics of continuum models often argue that their computational cost is too high to be used in large scale simulations (Cusatis *et al.*, 2006). This is only partially true, because these comparisons to lattice or particle models have been made on the basis of considering the same number and distribution of discretized particles. But in the case of models based on Voronoï/Delaunay diagrams, only the largest particles (say the upper third fraction) are considered explicitly in order to represent the same material and its behavior. So far, it has been shown that this seems sufficient, at least in the case of concrete, for capturing the main mechanical features under a diversity of loading situations either in 2D (López *et al.*, 2008; Rodríguez *et al.*, 2009) or 3D (Caballero, 2005; Caballero *et al.*, 2006). The performance of the model for its application to the analysis of coupled problems, including diffusion-driven phenomena with chemical reactions, is evaluated in this thesis.

The main differences between the various existing continuum models lie on the method used to create the geometries (see next sub-section), the way in which cracking is represented, and the meshing technique for the generated particle arrangement. Regarding the meshing techniques, aligned type of meshing is the most widely used, in which the finite element boundaries are coincident with materials interfaces and therefore there are no material discontinuities within the elements (Caballero *et al.*, 2006; Wang *et al.*, 1999; Wriggers & Moftah, 2006). Nevertheless, some authors prefer unaligned meshing, in which material interfaces may be positioned within a finite element (Zohdi & Wriggers, 2001). Additionally, structured (Caballero, 2005;) or non-structured meshing (typically based on a Delaunay triangulation, see e.g. Wang *et al.*, 1999, or Puatatsananon *et al.*, 2008) may be chosen, although non-structured meshes

often yield a larger number of degrees of freedom for meshing the same geometry, increasing the computational cost.

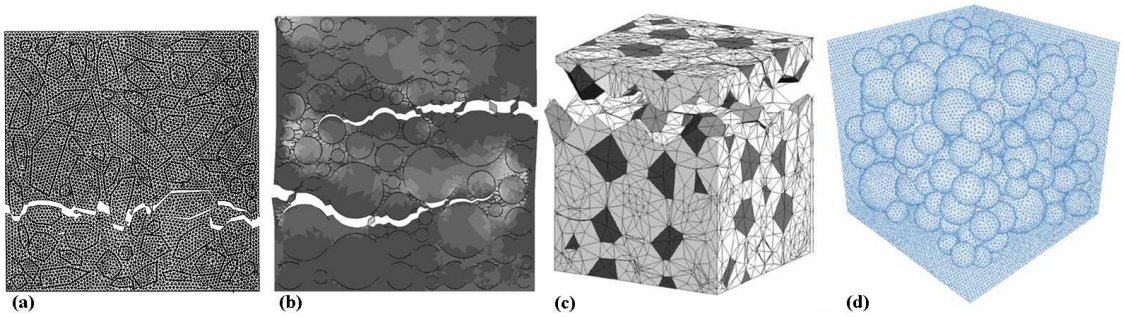

Figure 2.6. Different representations of continuum models. Crack patterns in a tensile test on non-structured meshes (a) from Wang *et al.*, 1999 and (b) from Tijssens *et al.*, 2001; (c) 3D crack pattern of a tensile test in a structured mesh (Caballero *et al.*, 2006); (d) 3D finite element mesh of concrete with spherical aggregates (Wriggers & Moftah, 2006).

2.2.4. Generation of geometries

Geometry generation is one of the most important points in a mesostructural simulation, since this procedure has to be able to capture the (desired) heterogeneous nature of the composite material, but at the same time lead to FE meshes that are not too large and well conditioned for numerical analysis. The most popular methods for generating the distribution of inclusions are the *take-and-place* method, with different degrees of sophistication (Wang *et al.*, 1999; Häfner *et al.*, 2003; Wriggers & Moftah, 2006), the *divide-and-fill* method (de Schutter & Taerwe, 1993), the *random particle drop* method (Vervuurt, 1997) and the Voronoï/Delaunay tessellations (Vonk, 1992; López, 1999; Wang *et al.*, 1999; Willam *et al.*, 2005). Another important issue is the shape of the particles. Highly detailed shape descriptions may be obtained by for instance adding sinus functions to an ellipsoid (Häfner *et al.*, 2003), although at a cost of prohibitive mesh refinement. Usually, spherical or ellipsoidal shapes are preferred when using the *take-and-place* or the *divide-and-fill* methods. On the other hand, irregular polygons naturally result from the Voronoï/Delaunay tessellations, which are closer in shape to natural aggregates, even though in some cases the resulting angularity is excessive. The first two methods allow for highly controlled aggregate size distribution to fit, e.g., a Fuller-type curve, either in 2D or 3D. This is not the case with the Voronoï polygons where, although the aggregate volume fraction as well as other geometrical properties may be perfectly controlled, the aggregate-size distribution is a result of the numerical random procedure, in general leading to similar-sized particles (of the same order of magnitude). Thus, the smaller particles are not explicitly discretized with this procedure. In contrast, the angular inclusion shapes obtained with the latter are somewhat more representative of concrete normal aggregates than the spherical or ellipsoidal ones resulting from the formers.

The use of circular inclusions makes it possible, in principle, to extract representative two-dimensional cross-sections from a three-dimensional arrangement of spherical particles *via* statistical analysis (Walraven, 1980; Schlangen, 1993). The problem is that the extraction of such a representative cross-section is not at all straightforward. Indeed, it is not clear if a *correct* 2D representation should be calculated as a result of cutting slices from a real 3D-arrangement (most of the 3D models proposed in the literature

have this capability, included the one presented in this thesis) or if on the contrary a statistical evaluation should be performed to obtain a correct size distribution instead (Häfner *et al.*, 2003). In their early work, Roelfstra and coworkers proposed to obtain representative 2D distributions by performing a large number of cutting planes on a 3D arrangement from which they extracted an average distribution for the corresponding size-grading curve (Roelfstra *et al.*, 1985), although it appears that this approach has not been followed in the literature.

The field of science dealing with the three dimensional interpretation of planar sections is called *stereology* (originally defined as the spatial interpretation of sections). It is based on basic geometry and probability theory. Although their fundamental principles have existed for more than 300 years (see Stroeven & Hu, 2006 for a historical review of the work by Cavalieri, Buffon and Cauchy), it is not until recently that this collection of tools for geometric measurements has started to be regarded as a real possibility for concrete researchers and technologists. This may explain why, to the author's knowledge, there is no single work dealing with mesostructural computational modeling of concrete behavior that considers stereology as a way to obtain more information on the geometries to be used (with the exception of Li *et al.*, 2003). The main principle of stereology associated with inferring geometrical properties of 3D composites from the observation of 2D sections is that *the volume fraction of inclusions is equal to the area fraction in a 2D section of the same composite* (Delesse, 1848). The validity of this principle depends only on the randomness of the plane with respect to the structure of the material, and not at all on the shape of the inclusions and their distribution within the matrix (Russ, 1986). It must be emphasized, however, that there is an important statistical problem of sampling: a considerable number of sections may be required to be analyzed in order to determine the mean volume fraction and the standard deviation. This means that a random section of the composite will not, in general, have an area fraction equal or close to the volume fraction. Nonetheless, the validity of this principle is of great relevance for two dimensional representations of real bodies. Unfortunately, the only quantity that may be extracted without any *a priori* hypothesis is the volume fraction. For all the other parameters, such as shape or size distribution, assumptions have to be introduced in order to extrapolate 2D observations to 3D representations (Moussy, 1988). Thus, the selection of a representative planar section remains a difficult choice.

This difficulty, together with the fact that two-dimensional simulations cannot capture the nonlinear three dimensional effects as bridging and branching of cracks in the out-of-plane direction (which is known to yield a more brittle material for the 2D case as compared to the real one) make the quantitative analysis of concrete in 2D a very hard task. Instead, and until 3D simulations are readily available, 2D simulations may be used for studying new phenomena and test new models at this scale. This is what is intended in this thesis. Although quantitative analysis is also pursued, 2D simulations have allowed us to focus on modeling aspects rather than on computational efficiency.

2.3. Crack modeling strategies

Modeling of crack formation and propagation has been a topic of major importance over the last 50 years and its progress has been notorious (Bazant, 2002; Cotterell, 2003; Gdoutos, 2005). Concrete mechanics has been an important driving force in this sense during the last three decades. This is in part due to the intricate nature of cracking

in concrete, where heterogeneities play an important role (Bascoul, 1996). Most models for crack formation and propagation rely on Fracture Mechanics principles, either classical linear elastic fracture mechanics (LEFM) or nonlinear fracture mechanics (NLFM). However, these principles are often superimposed onto a constitutive representation based on damage mechanics, plasticity theory or a combination of the previous. In practice, most cracking models may be grouped into two categories: the discrete crack approach and the smeared crack approach. Finally, the discrete crack approach followed in this thesis is based on the used of zero-thickness interface elements, the key ingredient of which is the constitutive model. All these aspects are reviewed in the following subsections. However, this chapter is not intended to review in detail classical continuum-type constitutive modeling such as damage or plasticity. For this topic, the avid reader is referred to the syntheses made in other theses of the group (López, 1999; Caballero, 2005) or to any advanced mechanics textbook.

2.3.1. Fracture principles: LEFM *vs.* NLFM

Given the quasi-brittle nature of concrete, at least under low levels of confinement, fracture mechanics appears as the most straightforward tool to represent its behavior. The first applications in this field considered LEFM, in which the strong assumption is implied that energy dissipation occurs only at the crack tip while the rest of the body remains linear elastic. However, this hypothesis is only reasonable when the zone affected by cracking is small enough as compared to the total structure, as in the case of fracture in dams, but in general its use is very limited in heterogeneous materials such as concrete, mortar or rocks. In reality, either in metals or concrete, nonlinear zones of varied size develop at the crack tip. The difference is that in ductile or brittle metals the material in the nonlinear zone undergoes hardening or perfect plasticity, whereas in concrete the material undergoes softening damage. This last kind of materials is called quasi-brittle since, although no appreciable plastic deformation takes place, the size of the nonlinear region is large enough and needs to be taken into account, whereas in brittle materials the size of the nonlinear region is negligible and LEFM applies (Gdoutos, 2005). This is one of the main differences between LEFM and NLFM, in which a finite fracture process zone (FPZ) exists, where the material behaves inelastically. This was first proposed for concrete by Hillerborg *et al.* (1976) with their celebrated Fictitious Crack Model (FCM), based on previous work in metals by Dugdale (1960) and Barenblatt (1962). Almost simultaneously, Bazant and coworkers (Bazant, 1976; Bazant & Oh, 1983) proposed the Crack Band Model (CBM), within the same line. The main difference between these two models is that the FCM considers that crack formation from a microcracked state may be reduced to a zero-thickness line, whereas the crack band model considers a finite width of the zone affected by cracking (figure 2.7). Moreover, NLFM has the advantage over LEFM of presenting a more neat formulation readily available for finite element implementation due in part to the stress singularity at the crack tip in the latter. This singularity in the stress field also requires highly dense meshes near this zone, limiting in this way its applicability to the cases where the direction of crack propagation is known *a priori*, or, alternatively, requiring advanced remeshing techniques.

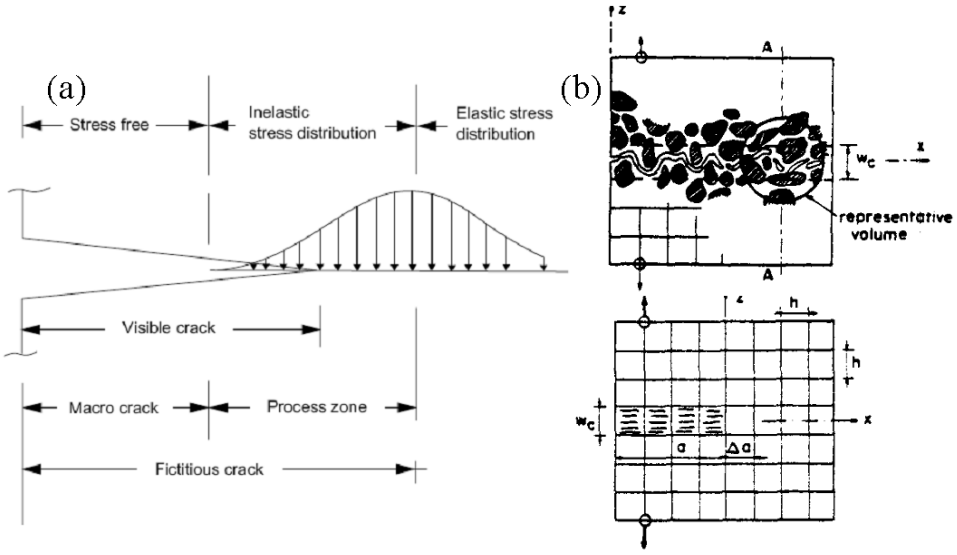

Figure 2.7. Cohesive crack concept *versus* crack band concept. (a) representation of the stress distribution ahead of the crack tip according to the cohesive crack model (from Gdoutos, 2005); (b) actual crack morphology and crack band model (from Bazant & Oh, 1983).

2.3.2. Discrete *vs.* smeared crack approach, and more recent developments

An essential feature of crack modeling techniques within the framework of NLFM is the selection of the crack representation, either by a *discrete crack approach* (Ngo & Scordelis, 1967), in which each crack is explicitly represented as a discontinuity in the continuum mesh, or a *smeared crack approach* (Rashid, 1968), in which cracks are considered to initiate and propagate within the finite elements representing the continuum. A complete review and a comparison of both approaches can be found elsewhere (de Borst *et al.*, 2004; López, 1999). Here, it is only intended to highlight some essential aspects of both techniques.

In principle, the discrete crack approach aims at capturing initiation and propagation of dominant cracks, whereas the smeared crack approach considers that many small cracks nucleate and finally coalesce into a dominant crack. Experience in the use of the discrete crack approach to simulate fracture of concrete at the meso-level (López, 1999; Caballero, 2005) has shown that this method is also suitable for simulating diffuse microcracking to finally form one or several macrocracks, including the typical bridging and branching effects and crack arrest by hard particles in cementitious materials under different loading situations. In the context of the discrete crack approach, the FCM (Hillerborg *et al.*, 1976), generally referred to as the cohesive crack concept, can be introduced naturally into a FE environment by using zero-thickness interface elements equipped with a fracture-based constitutive law (Carol *et al.*, 1997). Mesh bias may appear due to the fact that cracks are forced to propagate along element boundaries (Tijssens *et al.*, 2000; de Borst *et al.*, 2004). To overcome this defect, automatic remeshing may be implemented, although at the cost of considerably increasing the model's complexity and computational cost. A second possibility is introducing potential cracks in all lines in the mesh (or a sufficient number of them), which is the approach followed in the present work (Carol *et al.*, 2001). A research topic within the group aims at creating algorithms for introducing interface elements only when crack is about to initiate in a line, in order to optimize CPU time.

In the smeared crack approach, cracking is represented, together with the underlying continuum behavior, *via* an overall stress-strain law, i.e. *via* an equivalent constitutive model representing the average behavior of continuum plus cracks (see e.g. Rots, 1988). This approach, first advocated by Bazant & Oh (1983) under the name of the Crack Band Model for concrete, at first sight exhibits the attractive feature that it can be implemented into a FE code as any other standard constitutive law. This is probably one of the most important reasons that explain why smeared representations have usually been preferred in the literature. In fact, it can be shown that smeared crack models can be recovered from damage models, providing the damage variables are well identified (Pijaudier-Cabot & Bazant, 1987; de Borst, 2002; de Borst *et al.*, 2004). Moreover, this approach is also suitable for studying initiation and propagation of shear bands. However, the smeared approach leads inevitably to overall constitutive representations with softening, with the associated objectivity problems linked to mesh refinement. In fact, it has been shown that local models (in which the internal and field variables are defined locally in the mesh) exhibit strong mesh sensitivity. The solution of these problems requires a regularization of the finite element analysis, in order to account for the size of the finite elements through which the crack is propagating (de Borst, 2002), which is not straightforward at all. To this end, nonlocal models (Pijaudier-Cabot & Bazant, 1987; Tvergaard & Needleman, 1995) as well as special forms of nonlocal models with gradient enhanced terms have been proposed (Lasry & Belytschko, 1988; de Borst *et al.*, 1995; Peerlings, 1999). Although these models reduce some of the problems of local models, their implementation into a FE environment necessitates the definition of a new finite FE discretization for each increment where crack growth occurs (Peerlings, 1999). In contrast to smeared models, regularization of the mesh is not needed in the discrete crack approach, where the width of the crack line is zero. This allows the formulation of crack behavior to be done in terms of stresses and relative displacements of the crack faces, which is usually introduced *via* zero-thickness finite elements (see next section for references). Finally, it should be noted that also in the smeared crack approach a mesh bias could be introduced if cracks propagate in directions different from those of the mesh lines and no remeshing technique is used (Cervera & Chiumenti, 2006).

A final comment should be devoted to recent computational techniques developed to represent fracture. In the early 90's, continuum-based methods under the general name of *embedded discontinuity approach*, in which the deformational capabilities of the finite elements are enhanced, were proposed (e.g. Dvorkin *et al.*, 1990; Simo et al., 1993; Oliver, 1996). The purpose is to capture better the high strain gradients inside the crack bands in a more accurate way. Within this concept, two main possibilities have been explored (de Borst *et al.*, 2001). In the first one, the so-called *strong discontinuity appoach*, there is a discontinuity in the displacement field and localization takes place in a discrete plane (in 3D) (e.g. Dvorkin *et al.*, 1990; Simo *et al.*, 1993; Lotfi & Shing, 1995; Larsson & Runesson, 1996; Oliver, 1996). In the second approach, called the *weak discontinuity model*, energy dissipation occurs in a zone of a finite thickness with a strain that is different from that of the surrounding medium. The discontinuity is now introduced in the displacement gradient, being the displacement field now continuous (e.g. Ortiz *et al.*, 1987; Belytschko *et al.*, 1988; Sluys & Berends, 1998). However, these two approaches were later proven to be equivalent to smeared crack models, thus presenting many of their disadvantages, as e.g. the sensitivity of crack propagation to the direction of mesh lines (Wells, 2001).

A recently developed approach, introduced by de Borst and coworkers (Remmers *et al.*, 2003; de Borst *et al.*, 2004), is the *cohesive segments method*, which exploits the *partition-of-unity* property (Belytschko & Black, 1999) for the finite element shape functions. This method seems to eliminate mesh sensitivity and appears as a powerful tool to represent multiple cracks and bridging effects, including the advantages of both discrete and smeared crack approaches, although it is still under development and its application is still rather limited (de Borst *et al.*, 2004).

Another recent technique is the extended finite element method (XFEM), in which at the onset of cracking, nodal variables and displacement fields are duplicated in the elements implied, similar to overlapping elements with one layer attached to the continuum on each side of the crack (Jirásek & Belytschko, 2002).

Most these techniques, however, also inherit some problems from the underlying smeared approach they try to improve. On one side, the continuity of the crack is not explicitly enforced through elements, thus, to obtain a clean crack path, some underlying *ad-hoc* technique not based on fundamental mechanics principles ("tracking algorithm") is required to do the job behind the scene. On the other side, and as a consequence of that, only one or two (or at most a few) cracks can be handled at the same time, while the possibility of representing a bridging, branching and complex states of cracking remains limited.

2.3.3. Constitutive modeling for interface elements

There is a vast literature on constitutive modeling of crack initiation and propagation within the framework of the discrete crack approach represented by zero-thickness interface elements (usually formulated in terms of stresses and crack opening displacements). The most classical applications lie in the field of rock mechanics, for studying the behavior of existing discontinuities in rocks (Plesha, 1987; Gens *et al.*, 1990; Qiu *et al.*, 1993; Giambianco & Mroz, 2001), concrete mechanics (Stankowski, 1990; Carol *et al.*, 1997; Jefferson, 2002; Willam *et al.*, 2004; Puntel *et al.*, 2006), failure of masonry structures (Lourenço, 1996; Giambianco & Di Gati, 1997; Gambarota & Lagomarsino, 1997), seismic and safety analyses of arch dams (Hohberg, 1995; Carol *et al.*, 1991; Lau *et al.*, 1998; Ahmadi *et al.*, 2001; Azmi & Paultre, 2002) and delamination analysis of laminated composites (Schellekens & de Borst, 1994; Allix *et al.*, 1995; Chaboche *et al.*, 1997; Alfano & Crisfield, 2001; Jansson & Larsson, 2001; De Xie & Waas, 2006). Plasticity theory has been traditionally used in the early models (Plesha, 1987; Carol *et al.*, 1997; Lourenço, 1996; Schellekens & de Borst, 1994). In general, successful applications have been obtained at least under monotonic loading. The main disadvantage of plasticity applied to interface elements is its inability of representing the crack closure on unloading, although for some applications this is not a fundamental feature. Some authors have tried to keep the plasticity formulation format while introducing secant unloading in an *ad hoc* manner (Cervenka *et al.*, 1998; Schellekens & de Borst, 1994) for special cases of analysis. In this way, neither the consistency of the model nor energy conservation under elastic arbitrary loading paths is ensured. This has been remedied by different models within the framework of damage mechanics, thus yielding full recovery of the crack opening displacements on unloading (Allix *et al.*, 1995; Chaboche *et al.*, 1997; Alfano & Crisfield, 2001; Jansson & Larsson, 2001). The main drawbacks of damage models for interface elements are the numerical difficulties brought by stiffness recovery when passing from tension to compression and that they do not show the freedom of plasticity models to correctly represent dilatancy from phenomenological bases. In addition, cracking phenomena in concrete and other

quasi-brittle materials are often more complex and none of these two theories is able to represent the fact that on unloading the real behavior shows intermediate stiffness values between secant and elastic ones. This clearly indicates that a correct and sound representation from a physical point of view of the crack propagation and initiation with interface elements should consider a convenient mixture between plasticity and damage, as already proposed for continuum models (see e.g. Luccioni *et al.*, 1996 or Armero & Oller, 2000).

The work of Desai and coworkers and their *Disturbed State Concept* (Desai & Ma, 1992; Desai, 2001) is in this direction. They proposed to divide the total surface (in 3D) of a crack or interface into an *intact material* part and a *critical material* part, each one with its own constitutive behavior, thus differentiating from classical damage models. To compute the proportion corresponding to each part they introduced a *disturbance function* (going from zero to unity) depending on an internal variable. Unfortunately, in their work they only considered the case of shear-compression loading (plastic shear displacements are used as internal variable) and no reference is made to the tensile regime. A recent plastic-contact-damage model for interface elements has been proposed by Alfano and coworkers (Alfano *et al.*, 2006; Alfano & Sacco, 2006), enabling to obtain an intermediate crack opening and stiffness on unloading. The basic idea of this model is the coupling in parallel of a damage model and a plastic-contact model. The first one governs the proportions of undamaged material (with linear elastic behavior) and the damaged part, the latter with a sliding frictional behavior. Unilateral contact condition is treated in a special manner. Finally, the work by Jefferson and his *Tripartite Cohesive Crack Model* is worth mentioning (Jefferson, 2002). In this model, the nature of the problem is very well understood, although the resulting formulation is of high complexity due in part to its purpose of simulating fully experimental cyclic uniaxial loading of concrete specimens.

In the present study, a discrete crack approach with zero-thickness interface elements has been adopted throughout. The constitutive model is formulated within the framework of classical plasticity theory, introducing some NLFM concepts governing crack evolution, and is described in detail in the following sections. The constitutive law used in the interface elements is one of the most important aspects in the modeling of the mesostructure as proposed in this work, since it is here where most of the calculation time is spent (together with the calculation of the inverse of the global stiffness matrix), and also where the nonlinearity is introduced in the model. The main features of the interface element time-independent constitutive law will be introduced in the next section. In section 2.5, a complete formulation of the time-dependent constitutive law that accounts for the aging effect will be given.

2.4. Description of the model by Carol, Prat & López (1997)

2.4.1. Generalities

The constitutive model for interface elements that accounts for the aging effect has its origins in the formulation originally proposed in the early nineties within the research group (Carol & Prat, 1990), and later modified and improved in subsequent publications (Carol *et al.*, 1997; López, 1999; Carol *et al.*, 2001; Caballero, 2005; Caballero *et al.*, 2008). The model is formulated in terms of the normal and tangential stress components in the mid plane of the joint and the corresponding relative displacements:

$$\boldsymbol{\sigma} = [\sigma_N, \sigma_T]^t \tag{2.1}$$

$$\boldsymbol{u} = [u_N, u_T]^t \text{, with } ^t = \text{transposed} \tag{2.2}$$

It is based on the theory of elasto-plasticity and introduces nonlinear Fracture Mechanics concepts in order to define the softening behavior due to the work dissipated in the fracture process, W^{cr}.

The original model (Carol *et al.*, 1997; López, 1999; Carol *et al.*, 2001) exhibited the shortcoming of potential convergence problems due to a non-smooth plastic potential when changing from tension to compression (or vice versa), and to evolution laws with discontinuous derivatives in the limiting cases $W^{cr} = 0$ and $W^{cr} = G_F^I$ (or G_F^{IIa}, depending on the parameter considered). Moreover the integration algorithm was based on the mid-point rule and a non-consistent tangent matrix (López, 1999). In a later version (Caballero, 2005; Caballero *et al.*, 2008), some of these problems were fixed, by adopting evolution laws for the main parameters with continuous derivatives in all the range, a continuous plastic potential and a consistent tangent formulation (with quadratic convergence rate), with an implicit backward Euler scheme, based on the work by (Pérez Foguet *et al.*, 2001). The convergence rate is in this way greatly improved, at the expense of changing completely the plastic potential (which is in this case given by a second hyperbola).

In this work, a similar model to the original proposal in 2D is used (Carol *et al.*, 1997), with the difference that it incorporates the main aspects of the improved numerical framework (Caballero, 2005), namely the implicit backward Euler integration scheme with a consistent tangent matrix. Refinements have been introduced on the evolution laws and the plastic potential in order to improve the convergence without loosing consistency.

A comparison with different models for zero-thickness interface elements proposed in the literature, as well as a constitutive verification for different loading situations, may be found elsewhere (Carol *et al.*, 1997; López, 1999; Caballero, 2005; Puntel, 2004). In the following, the fundamentals of the model formulation are summarized.

2.4.2. Cracking surface and the elastic regime

The fracture surface (or yield surface) is defined by a hyperbola of three parameters in stress traction space, as it is shown in figure 2.8a, and can be expressed in the following way

$$F = \sigma_T^2 - \left(c - \sigma_N \cdot tan\phi\right)^2 + \left(c - \chi \cdot tan\phi\right)^2 \tag{2.3}$$

or, more conveniently for the numerical implementation, since only the branch of the hyperbola with physical meaning is kept (Caballero, 2005; Caballero *et al.*, 2008), as

$$F = -\left(c - \sigma_N \, tan\phi\right) + \sqrt{\sigma_T^2 + \left(c - \chi \, tan\phi\right)^2} = 0 \tag{2.4}$$

In this expression, the three parameters involved are χ (tensile strength), c (apparent or asymptotic cohesion) and $tan\phi$ (asymptotic friction angle). The initial values of the hyperbola parameters determine the initial configuration of the fracture surface, represented by curve "0" in figure 2.8c. Once the fracture process has started, the failure surface contracts due to the decrease of the main parameters, according to some evolution laws based on the work dissipated in the fracture process, W^{cr}. In order to

control the fracture surface evolution, the model includes two Fracture Mechanics-based parameters, namely the fracture energy in mode I, G_F^I (pure tension), and a second fracture energy in mode IIa, denoted as G_F^{IIa}, defined by a shear state under high compression level, so that dilatancy is prevented (schematically shown in figure 2.8b). In the case of a pure tensile test, the final fracture surface is given by a hyperbola with the vertex coinciding with the origin in the stress space (curve "1" in figure 2.8c). Under a shear/compression load, the final state, reached when $c = 0$ and $tan\phi = tan\phi_r$ ($tan\phi_r$ represents the residual internal friction angle), is defined by a pair of straight lines representing the pure residual friction state (curve "2" in figure 2.8c).

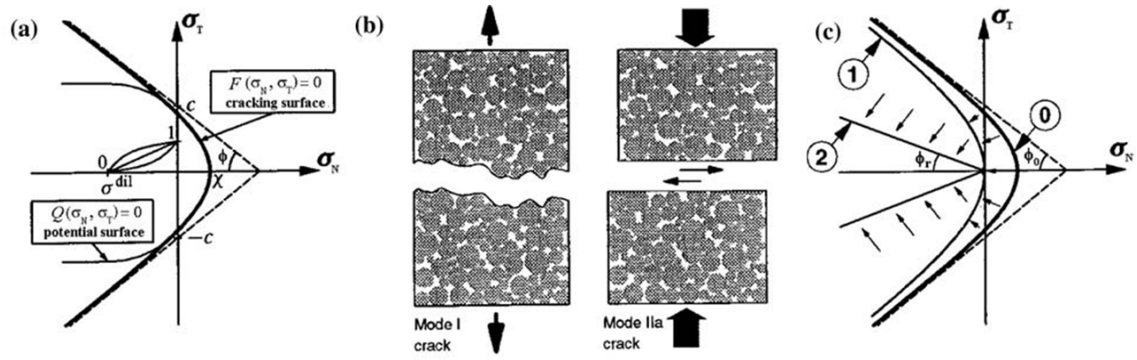

Figure 2.8. Crack laws: (a) hyperbolic cracking surface F and non-associated plastic potential Q; (b) fundamental modes of fracture; (c) evolution of cracking surface.

With the purpose of a clearer representation of crack patterns in mesostructural simulations (see e.g. Chapter 4, section 4.5.2.), it is useful to define the following states for the integration points:

- If $W^{cr} = 0$ and $F < 0$ then the integration point has never been loaded (and is not considered as an activated interface or Gauss point in the results);

- If $F = 0$ then the integration point is under plastic loading (and in the results it is considered as an active crack, usually assigned a red color);

- If $W^{cr} > 0$ and $F < 0$ then the integration point is under elastic unloading (and in the results is considered as an arrested crack, usually assigned a blue color).

Interface elements in the elastic regime, i.e. before cracking starts, should not add any extra elastic compliance. Therefore the elastic stiffness, defined by K_N (normal) and K_T (tangential) in a $2x2$ diagonal matrix (implying that there is no dilatancy effect in the elastic region), must be set as high as possible in order to minimize this extra compliance (representing a lower bound for the stiffness values). In this way, the elastic constants have the character of penalty coefficients which are necessary to calculate the interface stresses. The upper bound for these values must be set as a compromise between the added compliance and the numerical instabilities found for very high values (leading to very large trial stresses). Thus, it is important to know the minimum values for K_N and K_T (usually $K_N = K_T$ is considered) that have to be input in the model in order to have negligible elastic relative displacements of the interface element. Figure 2.9 shows a simple study of this type, in which two identical meshes at the meso-level of $10x10cm^2$ (shown in figure 2.9) have been loaded in compression in the elastic

regime, with the only difference that one of these meshes does not include interface elements (which will serve as a reference case) and the other does. The idea is to find the minimal values of the stiffness matrix of the interface elements that produce a global stiffness matrix of the mesostructure with a negligible difference with the reference case. It can be observed in figure 2.9a that for values of the parameter r (giving the relation of the interface stiffness to the most rigid continuum phase stiffness over the specimen length, in this case the aggregates with $E_{aggr.}$ = 70,000MPa, and the specimen length is 10cm) higher than roughly 1,000, the approximation is very close to the reference case. The same conclusion can be drawn from figure 2.9b. The following step has been to confirm that the numerical performance of the constitutive law is also satisfactory for these values, in the case of a nonlinear analysis.

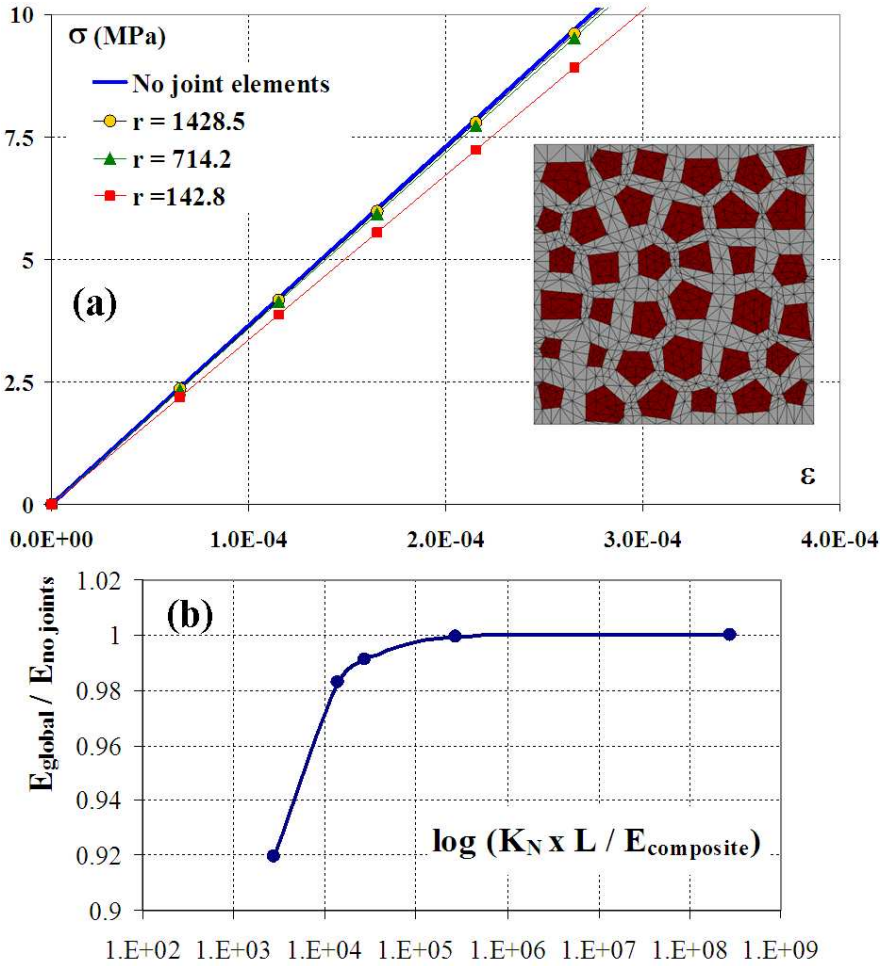

Figure 2.9. Influence of the interface element stiffness on the mesostructure global stiffness (corresponding to the mesh on the right, size is $10x10cm^2$): for different values of K_N and K_T, represented by the parameter r (relation between $K_N = K_T$ and the elastic modulus of the aggregates over the specimen length), and for the same case but without interface elements.

2.4.3. Plastic potential: flow rule and dilatancy

As in classical plasticity theory, an additive decomposition of interface relative displacements into a reversible (elastic, ***e***) and an irreversible component (***cr***) is assumed

$$\delta \boldsymbol{u} = \delta \boldsymbol{u}^{e} + \delta \boldsymbol{u}^{cr} \tag{2.5}$$

The inelastic part has to be defined in magnitude and direction, which is done by the introduction of a plastic potential Q and the plastic multiplier λ:

$$\delta \boldsymbol{u}^{cr} = \delta\lambda \frac{\partial Q(\boldsymbol{\sigma}, p)}{\partial \boldsymbol{\sigma}} = \delta\lambda \cdot \boldsymbol{m}(\boldsymbol{\sigma}, p) \tag{2.6}$$

where $\boldsymbol{m}$ is the flow rule, or partial derivative of the plastic potential with respect to the stresses. Typically, in heterogeneous materials such as concrete, crack paths exhibit irregularities due to a tendency to propagate through the weakest parts of the material (e.g. the interfacial transition zones). Due to this effect, shear stresses induce an aperture of the crack faces in addition to the sliding between them, phenomenon known as dilatancy. In order to determine the direction of this deformation (i.e. the dilatancy angle), a non-associated plastic potential Q is adopted (i.e. $Q \neq F$) and its derivatives with respect to stresses, denoted as $\boldsymbol{m}$, define the flow rule (figure 2.8a).

In the original formulation (López, 1999), an associated flow rule (i.e. $Q = F$) in tension and a non-associated one in compression was considered, in order to eliminate dilatancy for high levels of compression, determining a discontinuity in the flow rule when passing from tension to compression (or vice versa). As a consequence, the numerical convergence under tension-shear/compression-shear states was negatively affected. For this reason, a later proposal (Caballero, 2005) introduced a different hyperbola for the plastic potential (i.e. highly non-associated in the whole range of normal stresses, except in pure tension), maintaining in this way the continuity of the flow rule.

In this thesis, it has been decided to keep a relation between the fracture surface and the plastic potential as in the original model (and thus the relation between $\boldsymbol{n}$ and $\boldsymbol{m}$, being $\boldsymbol{n}$ the normal to the fracture surface), but extending the non-associativity also to the tensile regime. To this end, the plastic potential is made dependent on the energy spent in fracture (i.e. the internal variable, see next section), normalized with the fracture energy in mode IIa, yielding the following expressions

$$\boldsymbol{m} = \boldsymbol{A} \cdot \boldsymbol{n} \text{, with } \boldsymbol{n} = \frac{\partial \mathrm{F}}{\partial \boldsymbol{\sigma}} = \begin{bmatrix} tan\phi \\ \dfrac{\sigma_{\mathrm{T}}}{\sqrt{\sigma_{\mathrm{T}}^2 + \left(\mathrm{c} - \chi \cdot tan\phi\right)^2}} \end{bmatrix} \tag{2.7}$$

and where:

$$\boldsymbol{A} = \begin{bmatrix} 1 - \dfrac{W^{cr}}{G_F^{IIa}} & 0 \\ 0 & 1 \end{bmatrix}, \text{ if } \sigma_N \geq 0 \tag{2.8}$$

or

$$\boldsymbol{A} = \begin{bmatrix} \left(1 - \dfrac{W^{cr}}{G_F^{IIa}}\right) \cdot f_\sigma^{dil} & 0 \\ 0 & 1 \end{bmatrix}, \text{ if } \sigma_N < 0 \tag{2.9}$$

The term $\left(1 - W^{cr} / G_F^{IIa}\right)$ is continuous when passing from tension to compression (or vice versa), which has enhanced the convergence of the model in the critical tension-compression zone, and is consistent from a physical point of view, since a lower

dilatancy is to be expected as the material starts softening. Note that the non-associativity is not excessive in shear-tension, since the term $\left(1-W^{cr}/G_F^{IIa}\right)$ takes a minimum value of 0.9 when $W^{cr}=G_F^I$ (if $G_F^{IIa}=10G_F^I$). Also, the model is initially associated in tension, when the energy dissipated is zero, or throughout the loading process if there is no shear stress (i.e. under pure tensile load).

As mentioned above, a non-associated formulation is adopted for the plastic potential, so that dilatancy decreases progressively with the degradation of the joint (as described above) and also with the increase in the compression level ($\sigma \to \sigma^{dil}$ in figure 2.8a, as in Carol *et al.*, 1997). These effects are taken into account by a reduction of the normal component of the derivative of *Q*, as can be seen in expressions 2.8 and 2.9. Coefficient f_σ^{dil} accounts for the level of compression and takes the following form

$$f_\sigma^{dil}=1-S(\xi) \tag{2.10}$$

with

$$S(\xi)=\frac{e^{-\alpha}\xi}{1+\left(e^{-\alpha}-1\right)\xi} \tag{2.11}$$

and

$$\xi=\left|\sigma_N\right|/\sigma_{dil} \tag{2.12}$$

The scale function *S* provides a family of different evolution curves, depending on the adopted value of the shape coefficient α, which is defined in this case as $\alpha_{\sigma_{dil}}$ (figure 2.8a).

2.4.4. Internal variable

The model assumes that the evolution of the fracture surface is governed by one single history variable, given by the energy spent in fracture processes (W^{cr}) and is defined incrementally as (López, 1999; Carol *et al.*, 2001)

$$\mathrm{d}W^{cr}=\sigma_N\cdot\delta u_N^{cr}+\sigma_T\cdot\delta u_T^{cr}\text{, if } \sigma_N\geq 0 \tag{2.13}$$

$$\mathrm{d}W^{cr}=\sigma_T\cdot\delta u_T^{cr}\cdot\left(1-\left|\frac{\sigma_N\cdot tan\phi}{\sigma_T}\right|\right)\text{, if } \sigma_N<0 \tag{2.14}$$

in which δu_N^{cr} and δu_T^{cr} represent the increments of the relative displacements in the normal and tangential directions, respectively. These expressions imply that all the energy spent in the tension/shear zone comes from fracture processes, whereas in the compression/shear zone the contribution to W^{cr} is given by the work spent in shear, from which the pure friction is subtracted (Carol *et al.*, 1997; López, 1999).

2.4.5. Evolution laws for the hyperbola parameters

As previously outlined, the evolution of the fracture surface is governed by the energy spent in the fracture process. The degradation of the single hyperbola parameters is shown in figure 2.12 and formulated in the following (López, 1999; Carol *et al.*, 2001). For the case of the tensile strength, the evolution law reads

$$\chi = \chi_0 \cdot \left[1 - S\left(\xi_\chi\right)\right] \tag{2.15}$$

with:

$$\xi_\chi = \frac{W^{cr}}{G_F^I} \tag{2.16}$$

The evolution of the apparent cohesion is linked to that of tensile strength, in order to avoid inconsistent behavior in the tension/shear zone (López, 1999), by introducing a parameter *a*, representing the horizontal distance between the updated hyperbola vertex and its asymptotes:

$$c = \left(\chi + a\right) tan\,\phi \tag{2.17}$$

Parameter *a* varies between an initial value a_0 and zero, when $W^{cr} = G_F^{IIa}$, as can be deduced from figure 2.10.

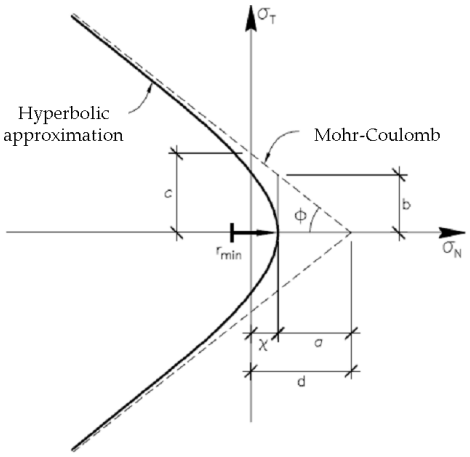

Figure 2.10. Fracture surface parameters, including parameter *a*.

Accordingly, the evolution of the apparent cohesion yields

$$c = \left[\chi_0 \left(1 - S\left(\xi_\chi\right)\right) + a_0 \left(1 - S\left(\xi_a\right)\right)\right] tan\,\phi \tag{2.18}$$

with:

$$\xi_a = \frac{W^{cr}}{G_F^{IIa}} \tag{2.19}$$

Finally, the evolution of the internal friction angle is given by

$$tan\,\phi = tan\,\phi_0 - \left(tan\,\phi_0 - tan\,\phi_r\right) S\left(\xi_\phi\right) \tag{2.20}$$

with

$$\xi_\phi = \frac{W^{cr}}{G_F^{IIa}} \tag{2.21}$$

and ϕ_r is the residual value of the friction angle, as shown schematically in figure 2.11.

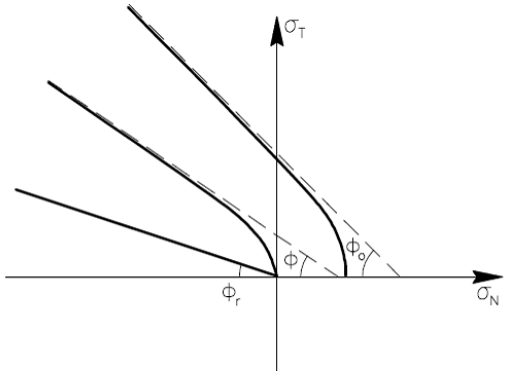

Figure 2.11. Schematic representation of the variation of the fracture surface when considering the evolution of the internal friction angle.

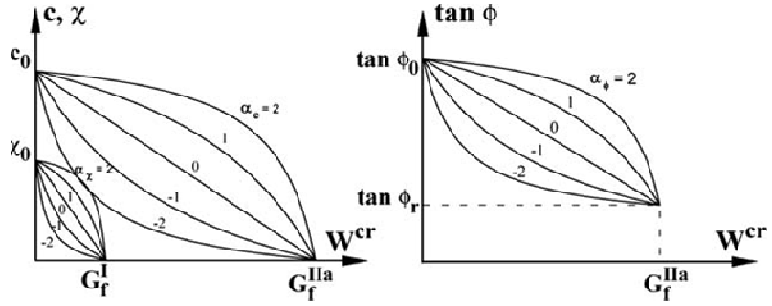

Figure 2.12. Softening laws for χ and c (left) and softening law for $tan\,\phi$.

It has also been suggested to generalize the parameter ξ_χ for the evolution of χ by the following expression (López, 1999):

$$\xi_\chi = \frac{W_1^{cr}}{G_F^I} + \frac{W_2^{cr}}{G_F^{II}} \;(a), \text{ with } G_F^{II} = (1-\beta)\cdot G_F^I + \beta \cdot G_F^{IIa} \;(b) \tag{2.22}$$

in which the work dissipated in fracture is split into two parts for mode I and mode II. Note that this expression requires the separation at every time of the different contributions to the energy spent in fracture, and thus necessitates the implementation of two internal variables. In this case, coefficient β (between 0 and 1) determines the dissipated energy needed to wear out the tensile strength, so that a zero value would be equivalent to the previous equation. However, for positive values a larger quantity of energy has to be dissipated to exhaust χ. A study of the effect of the parameter β at the local level (i.e. at the constitutive level) and at the global one (in the mesostructure) has been conducted in order to assess the impact on the global behavior. Results at the local level are presented in figure 2.13, in which the evolution of the apparent cohesion c is plotted against the dissipated energy. It can be observed that, since the evolution of c is attached to that of χ (eq. 2.18), there is a kink in the curve, whose position depends on the value of β (note that for $\beta = 1$ the discontinuity is eliminated). For $\beta = 0$, the tensile strength wears out fast, yielding a strong discontinuity in the derivative of c with respect to energy, yielding difficulties in the convergence. This is gradually fixed for increasing values of the β parameter. However, the global effect consists (as it would be expected) in a larger area under the stress-strain curve (i.e. a larger dissipated energy) with increasing value of β, even producing an increase of the peak stress of around 30% in a compression test. For this reason, in this work it has been decided to keep the original expression 2.16 for the evolution of χ.

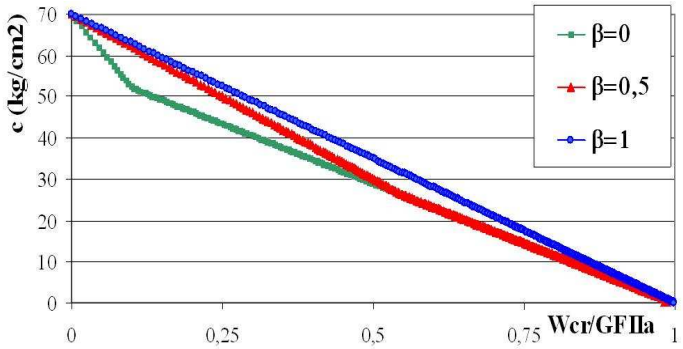

Figure 2.13. Evolution of the apparent cohesion as a function of dissipated energy (normalized with fracture energy in mode IIa), for different values of parameter β, at the constitutive level: the position of the kink in the curve depends on the value of β (χ_0 = 2MPa, c_0 = 7MPa, $\tan\phi_0$ = 0.6, G_F^I = 0.03N/mm and $G_F^{IIa} = 10G_F^I$).

2.5. Consideration of the aging effect in the constitutive model

In order to introduce in the model the effect of aging of concrete, represented by an increase of the strength with time, the evolution of the main parameters of the fracture surface with time is considered (χ, c), as well as the fracture energies G_F^I and G_F^{IIa} (the later assumed to be proportional to G_F^I). To this end, a phenomenological approach is adopted. A monotonic increasing function of the exponential asymptotic type is introduced, as shown in equation 2.23 and plotted in figure 2.14 for different values of the parameters (López *et al.*, 2005; López *et al.*, 2007).

$$f(t) = \mathrm{A} \cdot f(t_0) \cdot \left[1 - \mathrm{e}^{-\mathrm{k} \cdot \left(\frac{t}{t_0} \right)^{\mathrm{p}}} \right], \text{ with } \mathrm{A} = \frac{1}{1-\mathrm{e}^{-\mathrm{k}}} \tag{2.23}$$

In the previous equation, $f(t)$ and $f(t_0)$ are the values of the parameter considered at time t (age of the material) and t_0 (age at which the mechanical properties of concrete are referred to, usually considered to be 28 days), respectively, p is a shape parameter of the s-shape curve, and k is a parameter defining the relation between the final asymptotic value of the function and its value at time t_0. The effect of parameters p and k is shown in figure 2.14, plotting the term in brackets of eq. 2.23 as a function of time. As a result, the initial fracture surface (curve "0") given at a certain age will expand in time (to curve "1"), as shown in figure 2.15. It should be emphasized that in this first version of the model, the aging effect is decoupled from the moisture diffusion analysis, which is in fact a simplification of the real behavior. It is well-known that appropriate moisture conditions have to be present for aging to occur. A dried material will in general show no (or very little) increase in the mechanical properties with time. A future version of the model should definitely include this effect by e.g. considering an effective time in the exponential-type law, which would depend on the moisture level, as already proposed in the past (Bazant & Najjar, 1972). There are also more advanced models that introduce hydration and aging effects in a more sophisticated manner (see e.g. Cervera *et al.*, 1999).

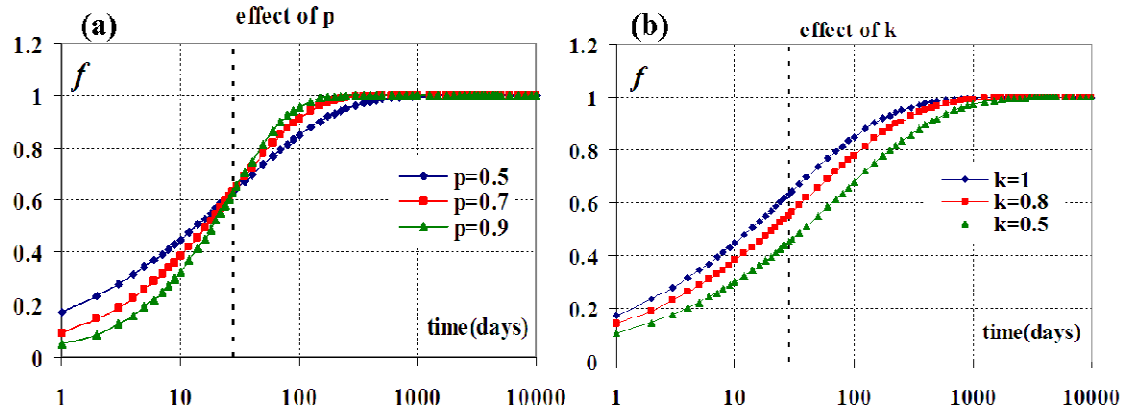

Figure 2.14. Evolution of the parameters relative to the value of function f (representing the term in brackets in eq. 2.24) at a sufficiently long aging period. (a) Effect of the parameter p on the s-shape of the function. (b) Effect of the parameter k on the value of f at t_0.(t_0 is equal to 28 days in the figure, and signaled with a dashed vertical line).

The consideration of the aging effect in the formulation allows for two counteracting effects to act simultaneously within the model: on one hand the fracture surface at a given time will be determined by the energy spent in the fracture process (if a dissipative mechanism is activated), leading to softening of the surface; on the other hand, the evolution of the main parameters in time (aging) will result in an expansion of the fracture surface. These features allow for the modeling of a much more complex resulting behavior of the joint element, since the updated fracture surface will depend on the resulting combination of the loading state and the time interval considered.

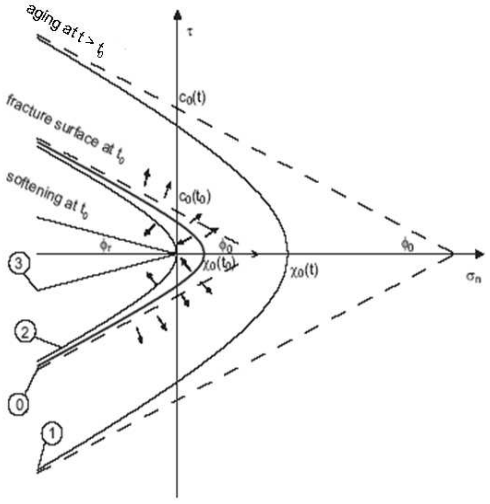

Figure 2.15. Cracking surface considering the aging effect: evolution with time and degradation due to energy spent in the fracture process.

2.5.1. Internal variable and evolution laws for the parameters

The energy spent in fracture processes (W^{cr}) has been defined in the previous section. In the present case, considering time-dependent parameters, the internal variable is more conveniently defined (incrementally) as

$$\mathrm{d}\xi = \frac{\mathrm{d}W^{cr}}{G_F^I(t)} \tag{2.24}$$

The evolution of χ and c is defined in terms of the work dissipated in fracture processes and the effect of time. In the case of the tensile strength, the expression is as follows

$$\chi = \chi_0(t) \cdot \left[1 - S\left(\xi_\chi\right)\right] \tag{2.25}$$

with:

$$\chi_0(t) = \mathrm{A} \cdot \chi_0(t_0) \cdot \left[1 - e^{-k_\chi \cdot (t/t_0)^{p\chi}}\right] \tag{2.26}$$

In the previous expression, $\xi_\chi = \xi_1$, with $\xi_1 = \xi_0 + \mathrm{d}\xi$, and $G_F^I(t)$ given by

$$G_F^I(t) = \mathrm{A} \cdot G_F^I(t_0) \cdot \left[1 - e^{-k_G \cdot (t/t_0)^{p_G}}\right] \tag{2.27}$$

The evolution law for c may be written as:

$$c = \left[\chi_0(t) \cdot \left(1 - S\left(\xi_\chi\right)\right) + a_0(t) \cdot \left(1 - S\left(\xi_a\right)\right)\right] \cdot tan\,\phi \tag{2.28}$$

in which

$$a_0(t) = \mathrm{A} \cdot a_0(t_0) \cdot \left[1 - e^{-k_a \cdot (t/t_0)^{p_a}}\right] \tag{2.29}$$

$$\xi_a = \xi_1 \cdot G_F^I(t_0) / G_F^{IIa}(t_0) \tag{2.30}$$

For the evolution of the internal friction angle ($tan\,\phi_0$ and $tan\,\phi_r$), the same law as in the time-independent version is assumed in this case (given by eq. 2.20), except that the internal variable is in this case given by

$$\xi_\phi = \xi_1 \cdot G_F^I(t_0) / G_F^{IIa}(t_0) \tag{2.30}$$

Note that for the case of the evolution of parameters defined within the range 0 to $G_F^{IIa}(t)$, such as $tan\,\phi$, the same internal variable is still used, since a constant relation in time between $G_F^{IIa}(t)$ and $G_F^I(t)$ has been adopted due to lack of experimental data (which is equivalent to assume equal values for the parameters of the evolution law in time given in eq. 2.23). Thus, in these cases the expression used is $\xi_1 \cdot G_F^I / G_F^{IIa}$.

2.5.2. Formulation

The hypothesis of additive decomposition of the relative displacements is still used in this case as starting point. Thus, the constitutive relation between stresses and relative displacements of the joint can be written as

$$\sigma_i = \mathrm{K}_{ij}^0 \cdot \mathrm{u}_j^{el} = \mathrm{K}_{ij}^0 \cdot \left(\mathrm{u}_j - \mathrm{u}_j^{cr}\right) \tag{2.31}$$

in which K_{ij}^0 is the (diagonal) elastic stiffness matrix of the joint. The irreversible component of the relative displacements is given by

$$\delta \mathrm{u}_j^{cr} = \delta\lambda \cdot \frac{\partial Q}{\partial \sigma_j} \tag{2.32}$$

with $\delta\lambda$ representing the plastic multiplier, which can be determined through the acting

loading state, *via* the well-known *Kuhn-Tucker* conditions:

$$\text{(a) } \delta\lambda \geq 0\,; \quad \text{(b) } \delta F \leq 0\,; \quad \text{(c) } \delta\lambda \cdot \delta F = 0 \tag{2.33}$$

If $\delta\lambda > 0$ then it corresponds to an elasto-plastic increment, and the Prager consistency condition allows the derivation of the following expression

$$\delta F = \left.\frac{\partial F}{\partial \sigma_i}\right|_{\lambda,t=const} \cdot \delta\sigma_i - \mathrm{H}\big|_{\sigma,t=const} \cdot \delta\lambda + \left.\frac{\partial F}{\partial t}\right|_{\sigma,\lambda=const} \cdot \delta t = 0 \tag{2.34}$$

in which:

$$\mathrm{H} = -\left.\frac{\partial F}{\partial \lambda}\right|_{\sigma,t=const} = -\frac{\partial F}{\partial \mathrm{p_i}}\frac{\partial \mathrm{p_i}}{\partial \xi_q}\frac{\partial \xi_q}{\partial \mathrm{u_j^{cr}}}\frac{\partial Q}{\partial \sigma_\mathrm{j}} \tag{2.35}$$

Parameter H is the plastic softening modulus, and p_i refers to the different parameters of the fracture surface. Note that equation 2.35 takes always a negative value causing the contraction of surface *F*, driven by the variation of the hyperbola parameters as a function of the internal variable. On the other hand, the term

$$\frac{\partial F}{\partial \mathrm{t}} = \frac{\partial F}{\partial \mathrm{p_i}}\frac{\partial \mathrm{p_i}}{\partial \mathrm{t}} \tag{2.36}$$

is characterized by the increase in strength as a consequence of the aging effect on the hyperbola parameters χ and *c*.

Combining eqs. 2.31, 2.32 and 2.34, the plastic multiplier can be expressed in the following way:

$$\delta\lambda = \frac{\mathrm{n_k K_{kj}^0 \delta u_j} + \dfrac{\partial F}{\partial \mathrm{p_i}}\dfrac{\partial \mathrm{p_i}}{\partial \mathrm{t}}\delta \mathrm{t}}{\mathrm{H} + \mathrm{n_p K_{pq}^0 m_q}} \tag{2.37}$$

Finally, the constitutive equation relating stresses and relative displacements of the interface element is written as

$$\delta\sigma_\mathrm{i} = \left[\mathrm{K_{ij}^0} - \frac{\mathrm{K_{ik}^0 m_k n_l K_{lj}^0}}{\mathrm{H} + \mathrm{n_p K_{pq}^0 m_q}}\right] \cdot \delta \mathrm{u_j} - \frac{\mathrm{K_{ij}^0 m_j}}{\left(\mathrm{H} + \mathrm{n_p K_{pq}^0 m_q}\right)}\frac{\partial F}{\partial \mathrm{p_r}}\frac{\partial \mathrm{p_r}}{\partial \mathrm{t}}\delta \mathrm{t} \tag{2.38}$$

The numerical implementation (with internal sub-stepping) of the model is analogous to the time-independent case, and may be found elsewhere (Caballero, 2005; Caballero *et al.*, 2008). The sub-stepping criterion adopted is equivalent to the one proposed in (López, 1999).

2.5.3. Constitutive verification

In this section, two fundamental examples of the model response at the constitutive (Gauss point) level are presented that illustrate the main features of the constitutive law in relation to the combined effect of the fracture degradation and the increase in strength as a function of time (López *et al.*, 2005b).

2.5.3.1. Shear/compression test

This test consist of applying a constant compression stress (-1MPa) in a first step, with loading ages of 28 and 280 days, and then gradually increase the shear relative displacement (maintaining the compression stress at a constant level). Figure 2.16

presents the results of this test in terms of shear stresses *vs.* shear relative displacements (and the corresponding fracture surfaces at different states identified with numbers 1 to 5 in the figure). For the cases of instantaneous loading, an increase of the peak value when loading at 280 days instead of 28 days can be observed. After the peak value, a softening branch is present, with a residual shear stress corresponding to the pure frictional effect.

A second set of simulations is calculated as follows: at the age of 28 days a similar loading history is applied to the joint, with the difference that, at 3 different points falling in the softening branch (i.e. 3 different tests), the loading increment is suspended until the material has an age of 280 days. At this time, the loading process is continued until a residual state is reached. In figure 2.16, it can be observed that an increase in strength is produced by the aging effect in the parameters $\chi_0(t)$ and $c_0(t)$ (e.g. between points 4 and 5 in the figure), until a second peak value is reached. In each case this value is lower than the values corresponding to the softening branch of the instantaneous curve at 280 days (at the same relative displacement), this difference being larger for increasing shear relative displacements. This effect is due to the damage-type nature of the internal variable of the model, which depends on the work dissipated in the fracture process and on the updated state of the fracture energy parameter involved (which is in turn a function of time.

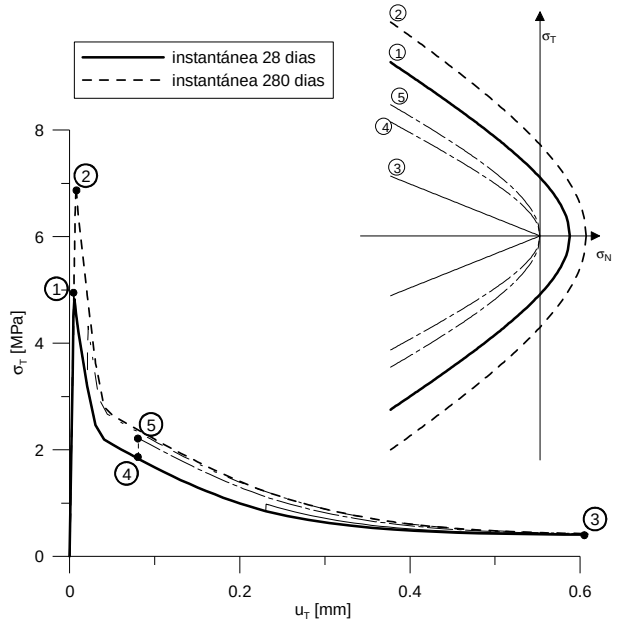

Figure 2.16. Constitutive behavior of the interface element for the case of a shear test under constant compression, in terms of shear stresses and relative displacements: effect of time.

2.5.3.2. Pure tensile test

In the second test, a positive normal relative displacement is incrementally imposed at the constitutive level (tension test). Analogously to the previous shear/compression case, two instantaneous tests at the ages of 28 and 280 days have been simulated, and the case of 28 days has been repeated, only that in the latter the loading process is interrupted at a certain level within the softening branch, as shown in figure 2.17. Once the age of the material reaches 280 days, the loading process is continued until an almost zero tensile strength. The constitutive behavior presents similar features to the previous example, as observed in figure 2.17. It has been observed that in order to

obtain the desired effect, the value of the parameter p for the tensile strength evolution must be lower than that for the fracture energy. Otherwise, the second peak after loading is continued at 280 days may be higher than the stress corresponding to the softening branch of the instantaneous loading at 280 days, leading to an inconsistent behavior from a physical viewpoint.

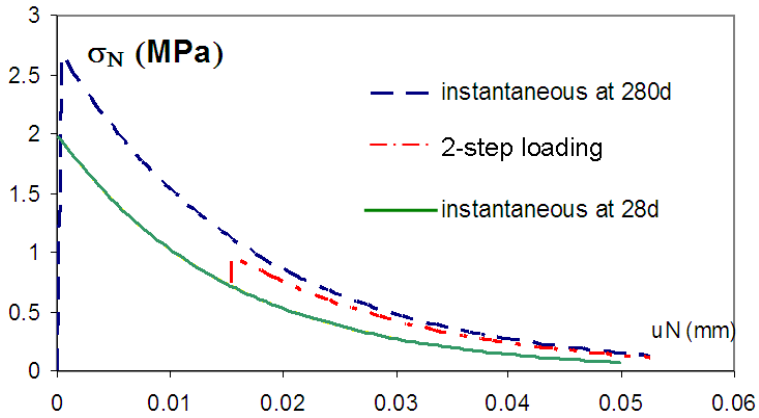

Figure 2.17. Constitutive behavior of the interface element for the case of a pure tensile test, in terms of normal stresses and relative displacements: effect of time.

2.6. Mesostructural continuum mesh generation in 2D

In this section, the stochastic procedure used throughout the thesis for generating the 2D geometries FE meshes (structured and aligned, see section 2.2.3.) that represents the mesostructure of concrete (or alternatively mortar) is described. The input data for such representation consist of fundamental parameters related to the mix design, such as aggregate volume fraction (or number of aggregates) and aggregate size and shape (rounded or with sharp edges), as well as some other parameters for controlling the randomness of the generation process. The same procedure, with some particular features in each case, has been extended, within the research group, to 3D mesh generation for concrete (Caballero, 2005), 2D analysis of trabecular bone (Roa, 2004) and to the problem of rocksanding production in oil wells in 2D (Garolera *et al.*, 2005). It should be emphasized that with this method only the largest aggregate particles are represented, which corresponds to approximately one third of the total aggregate volume for a typical sieve curve of a concrete with 75% aggregate volume fraction). The procedure is based on the Delaunay triangulation theory and the subsequent construction of the Voronoï polygons (exploiting the duality between these diagrams). The mesostructure is discretized in two phases: one represents the largest aggregates, and the second one is a matrix surrounding these aggregates, which in turn represents the mortar plus smaller aggregates as an equivalent homogeneous medium. Additionally, zero-thickness interface elements are introduced *a priori* in all the matrix-aggregate contacts and also within the matrix, in some predetermined positions, in order to represent potential crack propagation. The idea comes back to the work of Hsu and coworkers (Hsu *et al.*, 1963), which concluded that cracking in concrete starts at the aggregate-matrix interface (due to the fact that this bond is usually the weakest part of the material), and that the continuous crack trajectories propagate through the mortar matrix, serving as a bridge for the previous family of microcracks.

The procedure for the geometry and mesh generation is as follows. Starting from a predefined regular arrangement of points, the Delaunay triangle vertices (or,

equivalently, the geometrical centers of the Voronoï polygons) are obtained by a Monte Carlo perturbation of this regular scheme (figure 2.18). Each polygon obtained in this way will contain one (and only one) aggregate, generated by the contraction, in general non-homothetic, of the segments radiating from the geometrical center of the polygon to its vertices (Stankowski, 1990; Vonk, 1992; López, 1999). The contraction of each polygon is governed by the previously mentioned input data and optionally by a random shrinkage factor, allowing for obtaining a wider range of the final size distribution.

The following step is the addition of a rectangular frame, defining the total area and the dimensions of the mesh, which is external to the polygons before the shrinkage process, so that all the contracted polygons lie within this area. This allows for the generation of meshes with a matrix layer of mortar and small aggregates in the entire contour. This feature is particularly important when samples made with molds are to be simulated, since in these cases an outer mortar (or cement paste) layer is present, usually referred to as wall effect (see e.g. Kreijger, 1984 or Zheng *et al.*, 2003). This is in contrast to the core samples extracted from placed concrete, which in general cut the aggregates. This last case may also be simulated with the same procedure, only that in this case an internal frame is added to a larger geometry and all the elements falling outside this frame are eliminated. Figure 2.18 shows the first four steps followed in order to obtain the contracted polygons falling within an external frame.

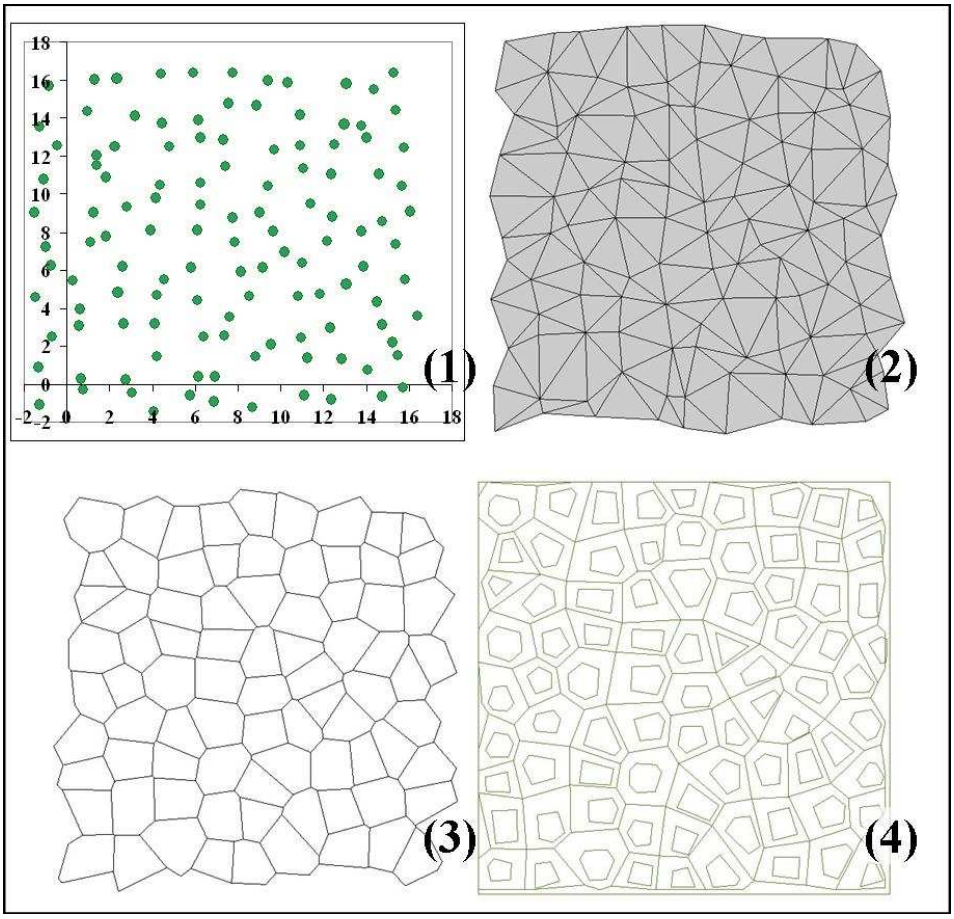

Figure 2.18. Stochastic procedure for the geometry generation of a mesostructure (mesh size is 15*x*15cm^2, with 28% aggregate volume fraction and maximum size of 15,7mm): (1) Monte Carlo perturbation of a regular arrange of points; (2) resulting Delaunay triangulation; (3) dual Voronoï polygons; (4) contracted Voronoï polygons within an external frame.

Next, the resulting geometry is divided into 'macroelements' for their subsequent discretization into finite elements (a standard or "structured" mesh solution is predefined for each type of macroelement, thus allowing a considerable simplification of the overall process). To this end, three types of macroelements are defined:

- Type 1 macroelements, formed by the lines linking the vertices between contiguous polygons (triangular and quadrilateral polygons may result, depending on the specific macroelement geometry);
- Type 2 macroelements, formed by the space left by the contraction of two polygons that shared one edge before contraction;
- Type 3 macroelements, defined by the contour formed by the external frame and the outermost aggregates, and type 2 macroelements.

In figure 2.19, the pretreatment of the final geometry for subdivision into macroelements is presented.

The macroelements and the aggregates are then discretized into continuum triangular finite elements, with a different arrangement for each type, as previously mentioned. For the case of aggregates, the final arrangement depends on the consideration or not of the possibility of aggregate cracking, and thus the addition or not of internal interface elements (as is the case for instance in high strength concrete simulations, see López, 1999). The discretization is shown in figures 2.20 and 2.21 for the different types of macroelements and aggregates, respectively.

The last step is the addition of the zero-thickness interface elements in predetermined positions. A first family of interface elements is added in all the aggregate-matrix contacts. The second family is generated between all the macroelement contacts and also through the diagonals of the types 2 and 3 macroelements (and the quadrilateral type 1 macroelements). As mentioned above, interface elements may optionally be added within the aggregates, with straight lines connecting the polygon vertices, as shown in the previous figure. The final arrangement of zero-thickness interface elements is shown in figure 2.22, together with the final FE mesh.

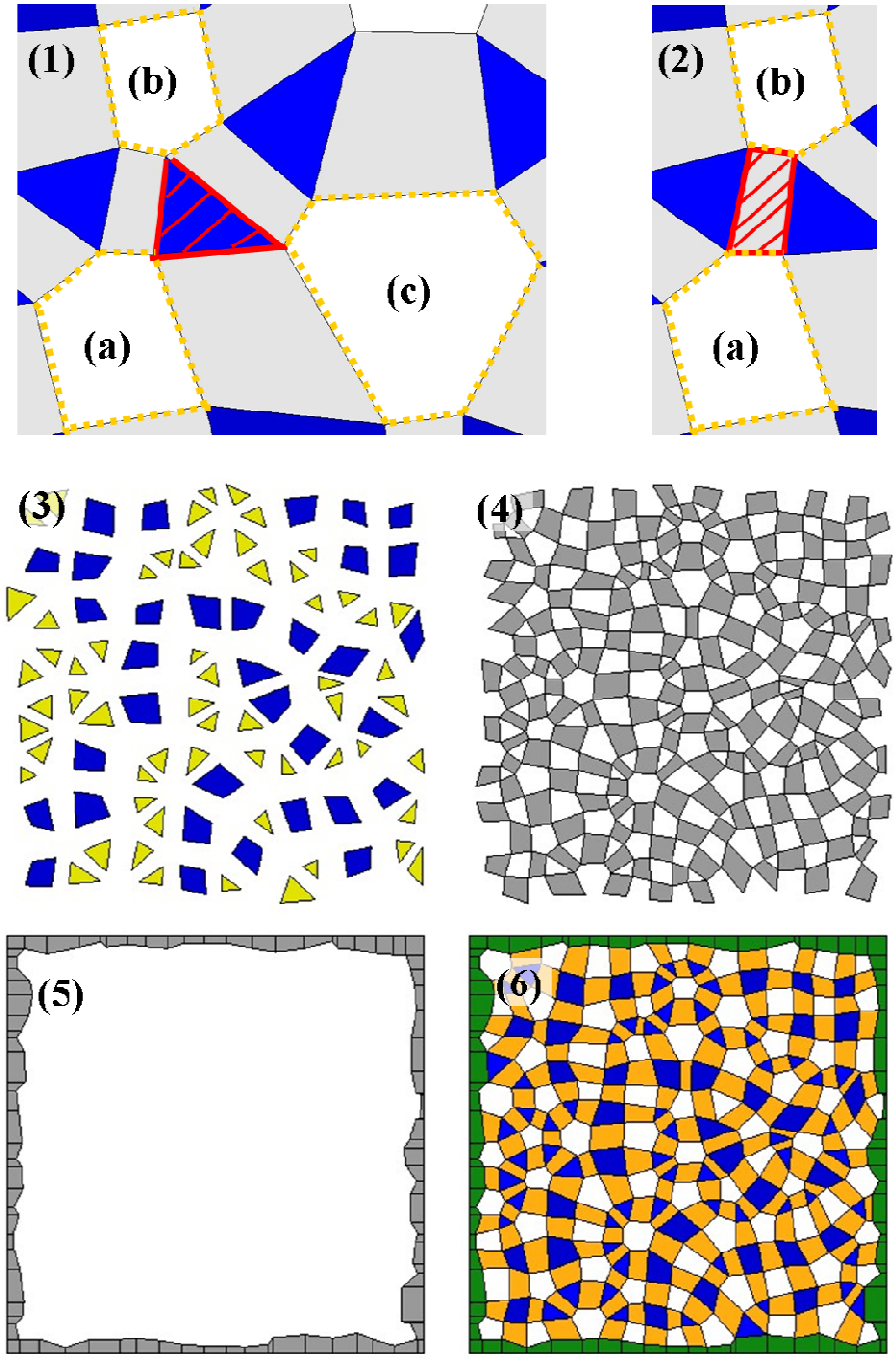

Figure 2.19. First step discretization of the geometry into ‘macroelements’: (1) detail of type 1 macroelement (shaded triangle) formed by aggregate vertices (a), (b) and (c); (2) detail of type 2 macroelement (shaded polygon) between two aggregate edges (a) and (b). Final arrangement of (3) type 1, (4) type 2 and (5) type 3 macroelements. (6) Final arrangement of all macroelements (white holes are the aggregates still not discretized).

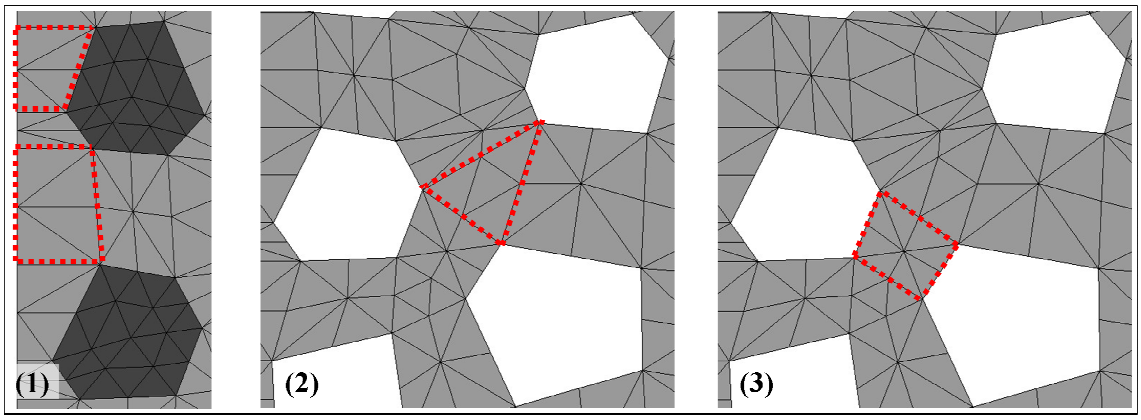

Figure 2.20. Final arrangement of ‘macroelements’: details of (1) type 3 (highlighted polygons), (2) type 1 (highlighted triangle) and (3) type 2 (highlighted polygon) macroelements.

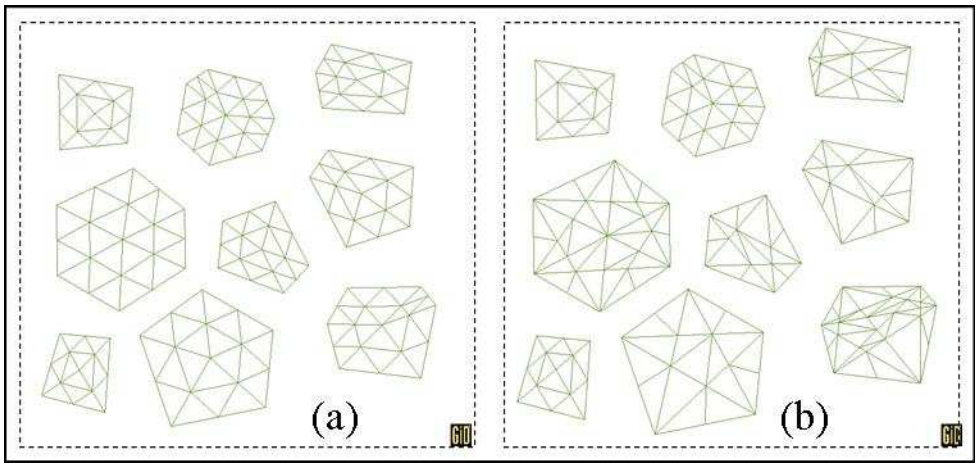

Figure 2.21. Discretization of the aggregates: (a) without and (b) with internal interface elements. Note that in the last case the assumption of fracture through the vertices of the aggregates is assumed by connecting vertices with a straight line of interface elements.

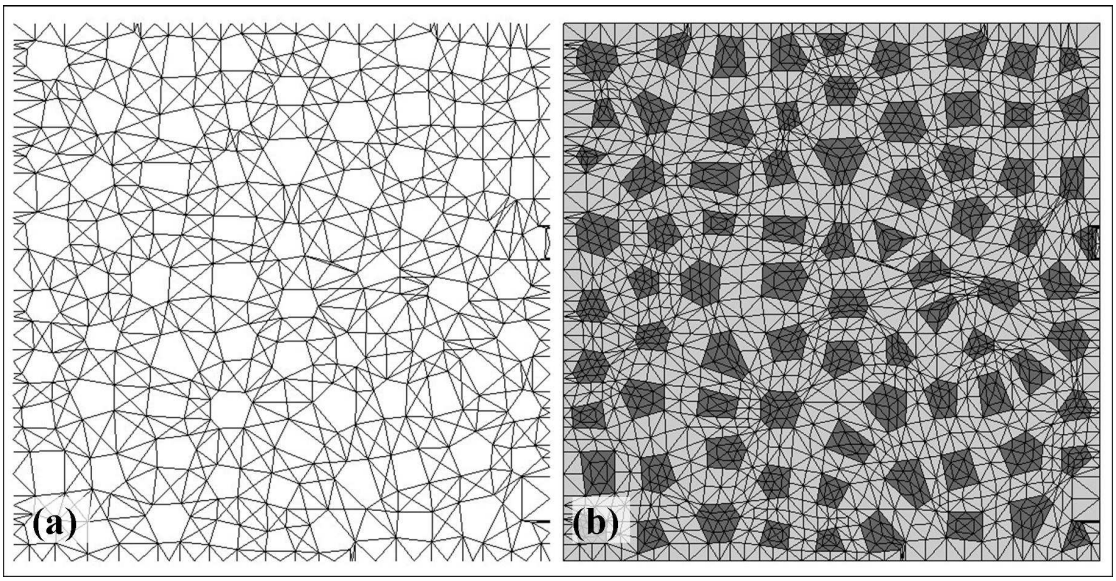

Figure 2.22. (a) Arrangement of zero-thickness interface elements. (b) Final FE mesh.

A significant effort has been devoted during the course of the thesis to enhance the performance of the mesh generation program in 2D, which had been initiated in recent years for the case of trabecular bone (Roa, 2004). In the present work, its extension to concrete (or mortar) mesostructures has been addressed, with the introduction of some noteworthy enhancements, including a complete restructuration of the *fortran* program and a greater control over the final geometry. More details of the work performed can be found elsewhere (Idiart, 2008). Focus has been made on the following features:

- more control of the aggregate shape, in order to allow for the generation of meshes with mono-size aggregates inscribed in circles of constant diameter while controlling the aggregate volume fraction (for the cases described in Chapter 4, section 4.5.2.);
- generation of post-processed information of the resulting geometry, with emphasis on the size distribution and the initial distribution of interface elements;
- generation of an external frame to the Voronoï polygons, for obtaining meshes with an external matrix layer (leading to the generation of type 3 macroelements), and an internal frame with interface elements (with the aim of capturing the stress state in the interior of a larger mesh); this has been a requisite in order to tackle the simulation of the Willam's test at the meso-level, which is on-going work within the group;
- introduction of an automatic procedure for refining specific edges of a given mesh with straight lines parallel to the surface, which is specially important for the diffusion-driven phenomena, studied throughout this thesis, in order to enhance the convergence and the quality of the results at the beginning of the diffusion process (see figure 2.23);
- implementation of a procedure for a systematic introduction of interface elements within the aggregates, to allow for aggregate fracture (and generation of a twin mesh without interface elements, for comparison purposes);
- procedure for the generation of notches of any desired size, allowing for the simulation of more complex cases as e.g. the Nooru Mohamed mixed mode test, the wedge splitting test (see figure 2.24), or the generation of C-shaped specimens (figure 2.25).

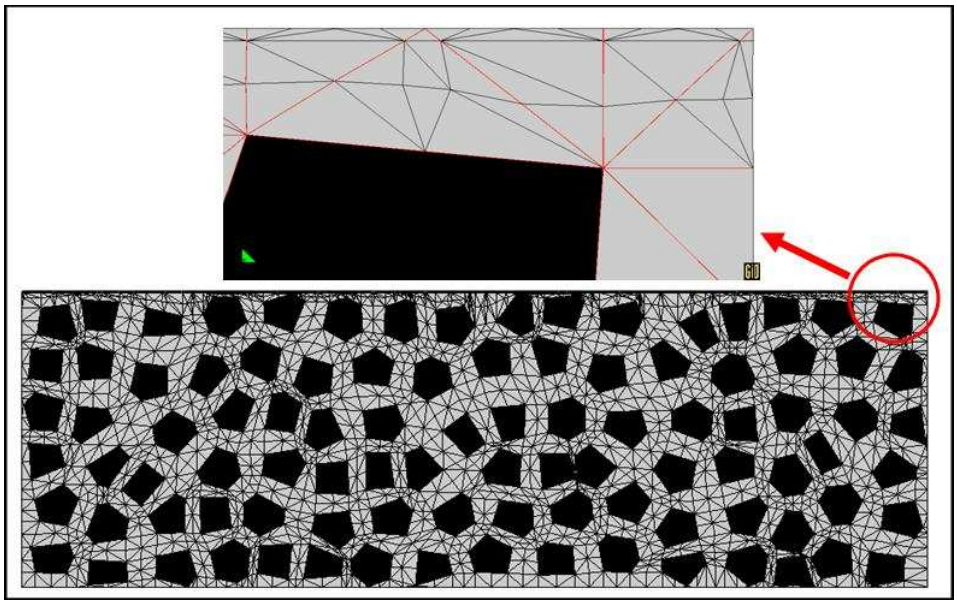

Figure 2.23. Detail of the mesh refinement near the upper surface.

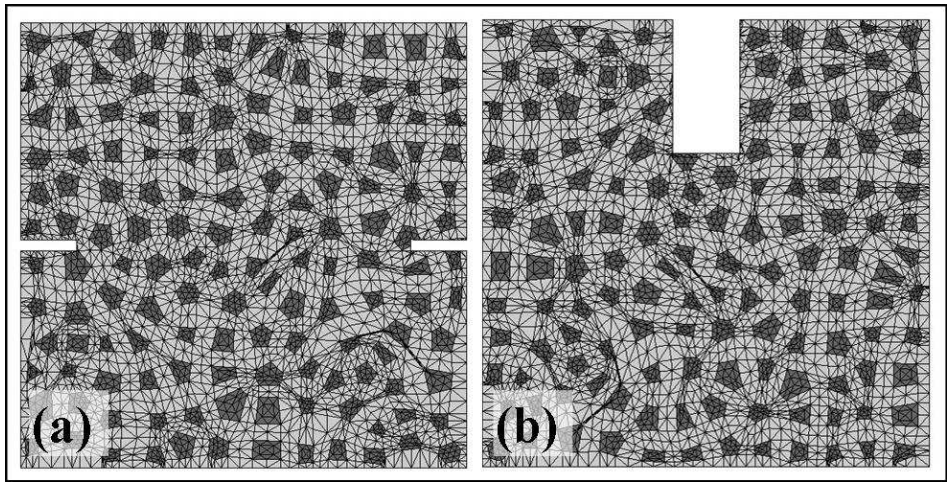

Figure 2.24. (a) 20*x*20cm^2 mesh with 25*x*5mm^2 notches on the left and right sides, and (b) 20*x*20cm^2 mesh with a 60*x*30mm^2 upper wedge.

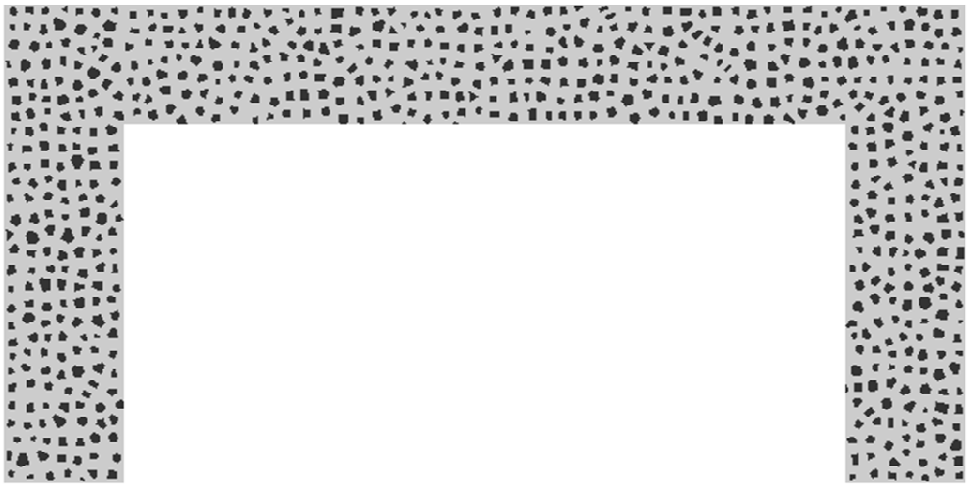

Figure 2.25. C-shaped specimen of 3cm thickness (length 24cm; height 12cm).

2.7. Description of the aging viscoelastic model for the matrix behavior

In order to simulate the time-dependent deformations in concrete at the meso-level, which will be described in detail in the next chapter, a basic creep model (under equilibrated moisture conditions) for the matrix phase of the mesostructure has to be introduced. A simple viscoelastic model with aging for the matrix behavior had been previously implemented (López *et al.*, 2003; Ciancio *et al.*, 2003), while aggregates are assumed to remain linear elastic and time-independent. Based on previous work by Bazant and coworkers (Bazant & Wu, 1974; Bazant & Panula, 1978; Bazant, 1982), the selected rheological model consists of an aging Maxwell-chain (figure 2.26a), which is equivalent to a Dirichlet series expansion of the relaxation function R(*t,t'*), dual to the usual compliance function J(*t,t'*), in which *t'* represents the age at loading. Rate-type models have fundamental advantages for numerical analysis, since it is no longer necessary to store the entire strain or strain history at each integration point. Because the matrix exhibits a time-dependent mechanism while the aggregates do not, the parameters of the Maxwell Chain for the matrix have to be set in order to produce the desired overall viscoelastic behavior corresponding to the concrete. In the present case, this adjustment is made with respect to the compliance function J(*t,t'*) given in the Spanish code (EHE, 1998; see also section 3.3.2. in Chapter 3) and shown in figure 2.26b. In figure 2.26b, the dashed line represents the compliance function for the matrix, the bold line the compliance function for a 28 days old concrete obtained as a result of the mesostructure (matrix plus aggregates behavior), and in the same figure, the J function for different ages, suggested by the Spanish code, is shown.

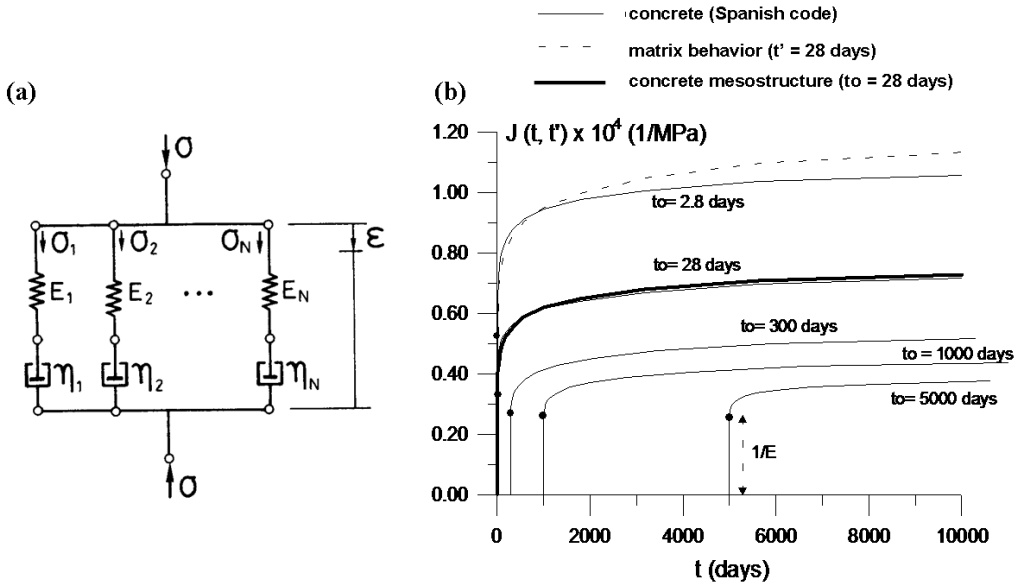

Figure 2.26. a) Maxwell chain scheme with springs and dashpots connected in series and each chain connected in parallel; b) inverse identification of basic creep law for the matrix behavior, showing the curve given by the Spanish code at different ages, and the behavior of the numerically generated microstructure at 28 days (dashed line for the matrix behavior and bold line for the mesostructure).

In the following section, some existing results of the overall behavior of concrete specimens including the effect of aging, in both matrix and interface elements, as well as basic creep in the matrix, are briefly outlined (López *et al.*, 2003; Ciancio *et al.*, 2003), in order to show the model capabilities.

2.7.1. Uniaxial compression test for different ages

To test the aging behaviour of the concrete model, a uniaxial compression test has been performed. In order to control the average stresses on the top surface of the specimen, an upper load platen, much stiffer than the concrete, has been included in the discretization for the creep test. The boundary conditions are shown in figure 2.27a. The displacements of the nodes on the bottom surface are constrained along the vertical direction, and the horizontal displacements are let free on the lateral edges, except on the bottom left edge of the specimen. The load is applied quasi-statically on the top platen in terms of prescribed vertical displacements and the test is repeated for specimens of different ages. The results are presented in figure 2.27b in terms of average stress and strain for different loading ages.

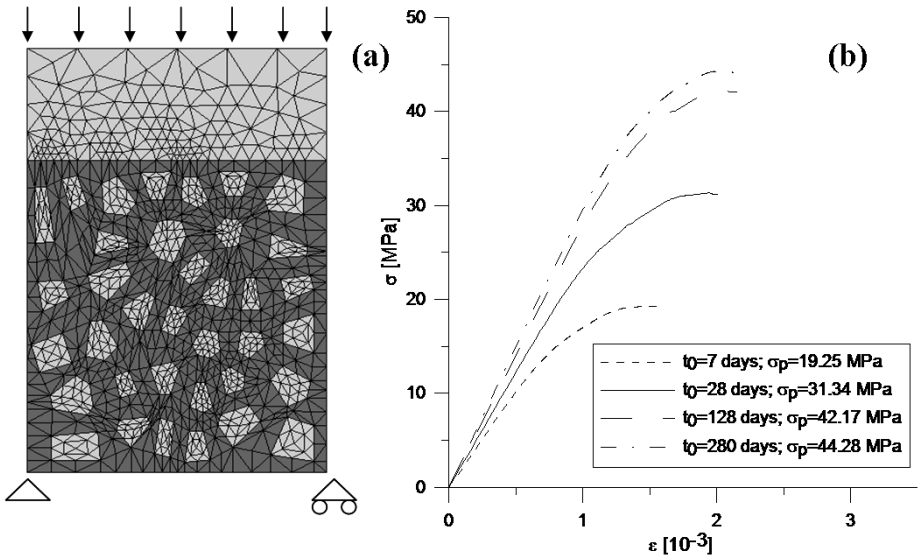

Figure 2.27. (a) Mesh used in the calculations with discretized loading platen and boundary conditions and applied load; (b) instantaneous uniaxial compression curves at various ages, and peak stress values.

As expected, the curves exhibit increasing strength values with the age of the material. This effect is due to the aging parameters of the interfaces that determine the overall peak value. The different elastic stiffness of the various curves is the result of the aging effect contained in the matrix model (Maxwell chain). It can be observed that the combination of the constitutive laws, described for interfaces and matrix, qualitatively reproduces the well-known effect of aging on the stress-strain curve of concrete.

2.7.2. Basic creep in compression

The same mesh and boundary conditions as before have been used for the basic creep test. The difference is that, in the present case the load is applied in terms of stresses on the upper platen rather than displacements. The test has been performed for two different specimens with ages at loading (*t'*) of 7 and 28 days. At age *t'*, a compressive load is applied up to a certain value, and then is kept constant during a period of 10,000 days, process which is repeated for different load values. The results are shown in figure 2.28 also in terms of stresses and strains for different loading ages.

The "continuous" curve on the left part of each diagram corresponds to the instantaneous compression test at age *t'*. The stress-strain path of each creep test follows

this curve up to the applied stress value, which then is kept constant. During this period, one can see the development of time-dependent strain, which corresponds to horizontal segments originating from the instantaneous stress-strain curve to the right. For stress levels higher than 0.3 to 0.5 of the quasi-static strength, cracking starts to develop during the constant stress period. This causes non-linear overall response with internal stress redistribution. These effects are more pronounced at higher stress levels (as depicted in figure 2.29 for 31 MPa of compression stress).

The classical isochrones curves are obtained connecting the states characterized by the same creep period (*t- t'*), as represented by the dashed lines in figure 2.28. The non-linearity of these curves, for load values greater than 40% of the peak, is captured by the model. Comparing two isochrones referred to the same (*t-t'*) period of the two different aged materials, one can notice larger strains for the younger specimen, in agreement with experimental behaviour.

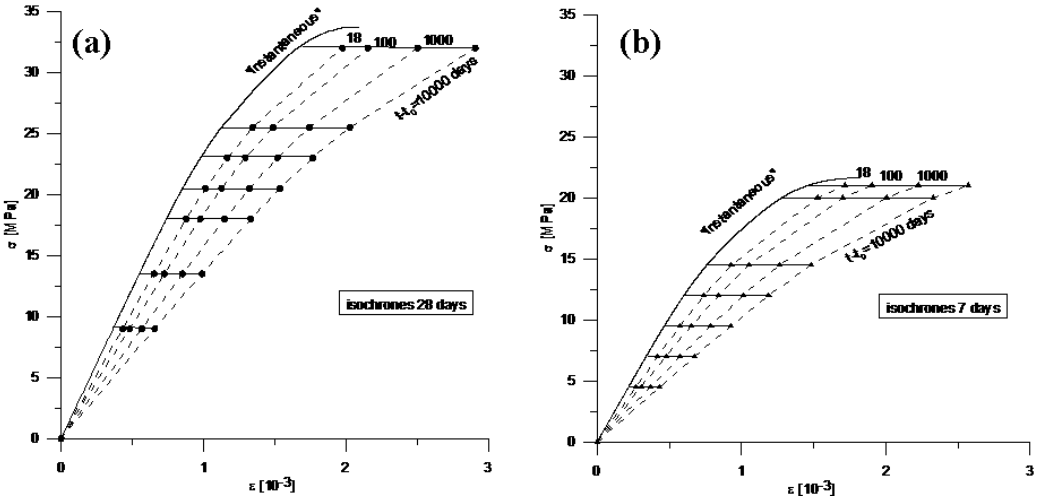

Figure 2.28. Basic creep isochrones at (a) 28 days and (b) 7 days.

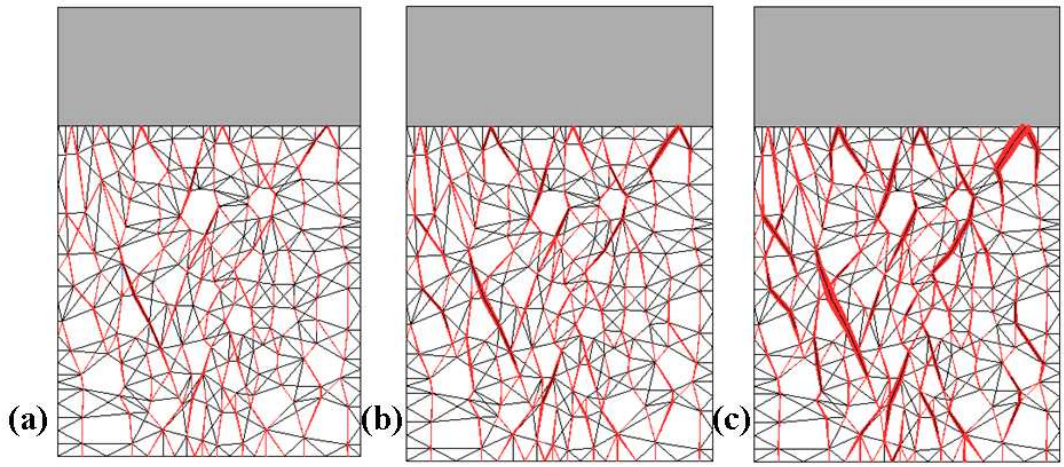

Figure 2.29. Crack evolution for a compression stress of 31MPa, at different *t – t'*: (a) 0, (b) 100 and (c) 10,000 days.